# ‘Simultaneous tracking of cell motility in liquid and at the solid-liquid interface’

Andrew L. Hook[1], James L. Flewellen[2,3,4], Irwin M. Zaid[4], Richard M. Berry[4], Jean-Frédéric Dubern[5], Alessandro Carabelli[1], Ricky Wildman[6], Noah Russell[7], Paul Williams[5*], Morgan R. Alexander[1*]

1. Advanced Materials and Healthcare Technologies Division, School of Pharmacy, University of Nottingham, Nottingham NG7 2RD, United Kingdom

2. Immune Receptor Activation Laboratory, The Francis Crick Institute, London NW1 1AT, United Kingdom

3. Division of Immunology and Inflammation, Department of Medicine, Imperial College London, London SW7 2A2, United Kingdom

4. Department of Physics, Clarendon Laboratory, University of Oxford, Parks Road, Oxford OX1 3PU, United Kingdom

5. Centre for Biomolecular Sciences, School of Life Sciences, University of Nottingham, Nottingham NG7 2RD, United Kingdom

6. Department of Chemical and Environmental Engineering, School of Engineering, University of Nottingham, Nottingham NG7 2RD, United Kingdom

7. Department of Electrical and Electronic Engineering, School of Engineering, University of Nottingham, Nottingham NG7 2RD, United Kingdom

* Joint Corresponding Authors

paul.williams@nottingham.ac.uk

morgan.alexander@nottingham.ac.uk

## 1. Abstract

To better understand key behaviors of living cells, such as bacterial biofilm formation, they must be observed above surfaces and at the interface between the surface and liquid medium. We have established a methodology for label-free imaging and tracking of individual cells simultaneously at both the solid-liquid interface and within the bulk, utilizing imaging modes of digital holographic microscopy (DHM) in 3D, differential interference contrast (DIC) and total internal reflectance microscopy (TIRM) in 2D as well as analysis protocols using a bespoke software package. We illustrate the power of this method by making detailed single cell measurements of *Pseudomonas aeruginosa* in the first minutes of their interaction with a glass surface, focusing on the role of the flagella stators, *motAB* and *motCD*. Using this new method we have determined their relative contributions to bulk and near surface motion for populations of cells at the single cell level.

## 2. Introduction

For many bacterial pathogens, swimming, swarming and twitching motility play key roles in host cell and tissue interactions, biofilm formation and virulence (1) and also enable micro-organisms to migrate towards nutrients or away from toxic substances (2, 3). In addition, flagellar and type IV pili not only facilitate bacterial movement but also play a role in surface sensing (4). Currently, the mechanisms by which individual cell behaviours translate to emergent, collective phenomena are not well understood. Therefore, the ability to collect data on a bacterial population at the single cell level will enable spatio-temporal dynamics to be revealed and to gain deeper understanding of the key signal transduction mechanisms connecting microbial motion with collective behaviours.

Single particle tracking measurements are important for studying a broad set of chemical and physical properties including diffusion, adsorption and desorption, or folding and unfolding (5). For bacteria, tracking in 3D allows for a complete analysis of bacterial movement and can be used to assess the trajectory of a bacterium approaching or leaving a surface. Early work following single cells determined the z-position by tracking the focal plane of a bacterium and recording x and y movements optically. This method can only follow a single cell at a time and is thus unable to record the movement of many cells in a population (6, 7). 3D volumes have also been imaged using optical techniques with narrow focal planes such as confocal microscopy to acquire z-stacks, but this approach is limited by low light transmission and consequently low acquisition rates. Alternatively, 'lookup' tables have been used to match the image of an object with reference images taken at known distances away from the focal plane of an object with fluorescent images (8), dark field microscopy images (9), and phase contrast images (10). This approach allowed the tracking of multiple cells simultaneously enabling identification of a range of motility patterns, such as the *run and tumble* motility identified for the peritrichous *Escherichia coli* and quantification of the swimming speed (10).

Most recently, 3D tracking of bacteria has been achieved using digital holographic microscopy (DHM) where the x, y, z-position of individual cells is encoded in recorded diffraction patterns and determined computationally after the acquisition of data (11, 12). For the monotrichous *Pseudomonas aeruginosa,* bulk growth medium swimming was analysed by DHM and motility patterns classified as *oscillation*, *meander*, *helix*, *pseudohelix* and *twisting* (13). The key advantage of DHM is its ability to observe the 3D trajectories of many cells in a bacterial population simultaneously; however, features such as their orientation and shape are difficult to ascertain from the holograms. A recent variant using a three laser setup permitted the use of DHM for determining bacterial volume and orientation throughout a 3D space; although, this approach has thus far only been demonstrated for the analysis of single bacterial cells released near the surface using optical tweezers (14).

To gain novel insights into the interplay between bulk cell motility and surface interactions, we have developed a novel multimode 2/3D microscope with interlaced acquisition of 2D surface differential interference contrast (DIC) or total internal reflectance microscopy (TIRM) images with 3D DHM. The spatial and temporal resolution of the DIC images at the surface were sufficient to allow the bacterial cell orientation to be determined, whilst TIRM imaging confirmed the close proximity to the surface (<200 nm) of near surface swimming cells. To enable imaging of a higher density bacterial population in 3D than is possible for DHM, we incorporated an optical relay to recreate the sampling area virtually, enabling it to be rapidly scanned in the z-dimension using a remote piezo-driven objective to avoid sample disturbance. A schematic of the multimode 2/3D microscope setup is shown in Figure 1a. Using this method we were able to determine the individual cell orientation and proximity to the surface as well as the 3D location of cells at low and high density over time for a single analysis chamber.

## 3. Results and Discussion

***Imaging of individual P. aeruginosa cells at the solid-liquid interface and in the bulk liquid***

To achieve DHM imaging a sample was illuminated by a coherent light source (685 nm laser). DIC imaging required illumination of the sample by a polarised light source with the use of Wollaston prisms above and below the sample. Use of the prisms did not adversely affect DHM image quality. TIRM imaging required illumination of a laser light source from below with the use of a 50% mirror. All these requirements were met without interfering with the other imaging modes, thus, multimode acquisition could be achieved by modulating the intensity of the different illumination sources under computer control. The limiting factor in the time resolution of bacterial motion capture was the frame rate of the camera, which in this case was 100 Hz.

*P. aeruginosa* was grown to the log phase in lysogeny broth (LB) to maximise the number of motile cells. The bacteria were injected into a sample chamber consisting of two glass coverslips sandwiched together using double-sided tape and sealed with a hydrocarbon grease immediately after introduction of the LB culture (volume dimensions 18×5×0.1 mm Figure 1b). Bacteria were observed to undergo cell division within the chamber for 4-6 h until reaching the stationary phase. To enable the assessment of

bacterial motility, interlaced capture of either 2D DIC or TIRM at the surface and 3D DHM images was conducted at 41.7 Hz (total frame rate) within 5 min of bacterial cells being added to the sample chamber (Figure SI3). At this frame rate bacterial fluctuating motion was undersampled (body and Brownian motion) but oversampled in terms of directional motion (Figure SI4). After data acquisition, bacterial trajectory generation was achieved using bespoke Matlab scripts (DHMTracking and StackMaster). Using this approach, bacterial trajectories could be determined both within the bulk (Figure 2a) and at the glass surface-medium interface (Figure 2c-d). At the surface using DIC, the orientation of the bacterial cells could also be determined to establish whether a cell was orientated in the direction of travel and if cells were attached via their long axes or poles (Figure 2b). TIRM allowed the surface proximity of cells to be measured since objects were only detected up to the penetration depth of the evanescent wave, set to 200 nm by controlling the incidence angle (Figure 2d).

Single cell bacterial trajectories were determined using DHM (Figure 2a) at cell population densities of up to $1.7 \times 10^4$ cells/µL, above this, overlapping interference patterns inhibited holographic reconstruction. To measure the 3D distribution of cells at higher populations we used the remote image relay to acquire a series of DIC images separated in the z-axis, referred to as *z-stacks*. Analysis of the z-stack data enabled the position of each bacterium to be determined at a population density of $3.7 \times 10^5$ cells/µL, greater than an order of magnitude improvement over holography, with a maximum population density within any one image of $8.0 \times 10^5$ cells/µL This enabled the growth of a *P. aeruginosa* cell culture to be determined over 4 h at the single cell level (Figure 2b). Objects that were vertically contiguous for adjacent frames were attributed to a single bacterium and the position of the cells was determined as the zero-order moment of inertia calculated from all pixels taken for combined objects. An example for a single z-stack is shown in Figure SI5-6. We employed a z-spacing of 1 µm in order to ensure that we did not omit bacterial cells when imaging (typical cell dimensions = 2 × 5 µm, depth of field at 60× magnification NA = 1.4 ≈ 0.6 µm). Over a z-range of 100 µm and a maximum imaging rate of 100 Hz, this meant that the maximum acquisition rate using the DIC z-stack was 1 Hz. Although useful for determining the cell population density and distribution, the lower acquisition rate of this approach compared to DHM made it impractical for tracking fast swimming bacterial motion since for accurate tracking; bacteria should not travel further than their dimensions per frame, thus, limiting this approach to cell motions slower than 5 µm/s.

### *3.1. Characterisation of bacterial trajectories*

*P. aeruginosa*, a Gram-negative rod-shaped cell with a single polar flagellum employs a number of different mechanisms for moving through liquids and across surfaces. These include flagella-mediated swimming, spinning, near-surface swimming and swarming, type IV pili-mediated twitching (crawling and walking), gliding (active movement without the use of flagella or pili), and passive movement through the use of surfactants termed sliding (15, 16). In this study we focussed on swimming motility trajectories associated with flagellum-driven movement that were typically observed at speeds greater than 10 µm/s.

A number of different bacterial swimming trajectory phenotypes were visually observed within individual *P. aeruginosa* populations. Relatively straight trajectories with cells travelling at high speeds were seen, which we will refer to as *runs* after the convention of Berg et al (17) (Figure 3a). Cells were found to be swimming parallel to the surface termed *near surface runs* (Figure 3b), a phenomenon that has been assigned to various mechanisms including hydrodynamic interactions, Brownian motion and surface contact (9, 18, 19). Visual inspection of the tracks indicated that near surface runs had a greater incidence of directional change events than those observed in the bulk where trajectories were straighter for longer. Moreover, we observed circular trajectories when bacteria were travelling at the surface consistent with previous studies (20). This near surface run curving phenomenon has previously been attributed to flagella-mediated surface interactions (20). Using TIRM, we were able to show that the bodies of near surface migrating bacteria were swimming parallel to the surface at a distance of less than 200 nm (Figure 2c), a separation substantially shorter than the typical length of a bacterial flagellum (≈ 5 µm, Figure SI7) (21). Through interlaced capture of DHM and TIRM imaging, the centre of mass of the bacteria (as determined by DHM) and the centre of mass of the contact point (as determined by TIRM) were compared (Figure 2c). The majority of cells (75.4%) exhibited a similar centre of mass and contact point, consistent with cells swimming aligned to the surface. In some cases, bacteria swam with the surface contact point either at the front pole (20.4%) or at the rear pole (4.2%) of the cell defined by its direction of travel, consistent with the cell swimming front pole up or down. We note that using our method it is likely that the number of cells swimming front pole up or down may be underestimated due to uncertainty of the z-position of the bacteria; the measurements presented assume that the bacteria are in contact with the surface. This observation of monotrichously flagellated *P. aeruginosa* differs from observations of the swimming of the peritrichously flagellated *E. coli*, where all cells were found to be swimming with the front pole down to the surface (14).

In the bulk, an alternative class of swimming trajectory than runs was observed, where the movement of the bacteria was slower and characterised by frequent reversals of swimming direction, a phenomenon assumed to be caused by reversals of flagella rotation directional (Figure 3c), termed *oscillating* after the classification applied by Rosenhahn et al (11). These bacterial cells were travelling at a reduced speeds of 12 ± 5 µm/s, substantially slower than the cells exhibiting run trajectories at 59 ± 4 µm/s. Notably, we did not observe *oscillating* cells at the surface, likely because the constraints of the proximal surface restricted the directional change of the cells upon flagella reversal. *Near surface runs* were slower and exhibited more frequent changes in direction than bulk *runs*, which we term *rambling,* a motion that has not previously been reported. *Rambling* at the surface did not include the high frequency of directional reversals seen in the bulk (>90 degree) for oscillating cells.

Some cases were observed where *P. aeruginosa* trajectories were reminiscent of peritrichously flagellated *Escherichia coli* run-and-tumble patterns (22), whereby a straight 'run' path was interspersed by a high frequency (2 Hz) of reversal events before the

bacteria recommenced a run trajectory (Figure SI8). The average reversal rate observed in the bulk population was 0.5 Hz. We observed no change in the orientation of the bacterial body for surface reversal events (where the change in direction exceeded 120° - Figure 3d) observed at the glass surface (Figure 3e), consistent with these reversal events being caused by a change in flagellum rotational direction inducing a reversal of the bacterial direction of travel without reorientation of the bacterial body (13). To observe this more closely, we imaged cells using a third of the camera's chip size enabling a higher acquisition rate of 333 Hz. At this higher frame rate we were still unable to observe any reorientation of the bacteria (Figure SI9). Moreover, equipping the microscope with a fluorescence filter set enabled the use of total internal reflectance fluorescence (TIRF) imaging in order to visualise flagella through the use of fluorescent staining. Using this approach, flagella were readily observed at both the leading and trailing end of bacteria before and after surface reversal events (Figure SI10), showing that *P. aeruginosa* cells are able to use their flagella to both push and pull, consistent with previous observations for monotrichous bacteria (23-25). We observed no statistical differences in the speed of bacterial trajectories before or after a reversal event (Figure SI11).

Stationary cells at the surface were found attached either horizontally or vertically (long-axis or pole attached). Long-axis attached cells were identified from DIC images where the distinct rod-shape of the bacteria was observed and remained stationary throughout the duration of an image sequence with no change in the centre of mass of the cell (Figure 2b). In contrast, pole-attached bacteria were observed to be smaller and circular in appearance and small deviations in the cell's centre of mass were observed as the cell wobbled on a single attachment point (Figure 2b). In some cases, polar attached cells were observed to be spinning due to the flagella being fixed to the surface whilst the bacteria body remained free and able to rotate, a phenomenon observed previously (15) (Figure SI12).

### *3.2. Exploring the respective contributions of the two* P. aeruginosa flagellar *stators to swimming motility*

The motility trajectories of *P. aeruginosa* are of interest due to the prevalence of this opportunistic pathogen in human disease (11, 26-28). The bacterial flagellum is also associated with bacterial surface sensing and plays a key role in detection of a surface during the early stages of biofilm formation (29). The *P. aeruginosa* flagellum, unlike most other bacterial species, is driven by two (rather than one) stator complexes termed MotAB and MotCD. These are the static elements of the bacterial motor that provide energy to turn the flagellum and to control speed and torque (30). Either MotAB or MotCD is sufficient for swimming but the two stators make differential contributions to swarming motility and biofilm formation (31-34), since it has been observed that deletion of *motCD*, but not *motAB*, renders *P. aeruginosa* incapable of swarming at an agar concentration above 0.5 % (a collective surface movement observed for certain bacteria) (34). The specific contributions of the two stators to individual bacterial cell trajectories, to our knowledge, has not previously been reported. We therefore utilised the multimode 2D/3D microscope to study trajectory phenotypes for wildtype and isogenic *motAB*, *motCD* and *motABCD* deletion mutants to explore the contribution of the

two stators to swimming motility. For five biological replicate wild type *P. aeruginosa* and *mot* mutant cultures, bacteria were tracked over a 2.4 s interval as shown in Figure SI13. As expected, the *motABCD* mutant was non-motile (31-33) and therefore not analysed further.

We investigated whether quantification of the cell trajectories could be used to categorise the different forms of cellular movement that were readily apparent on visual inspection of cell tracking videos. Cell tracks analysed and quantitatively characterised using instantaneous speed, total displacement, and their mean square displacement (MSD) over the time range ($\delta t$) of 50 to 1000 ms (Figure SI14). The slope of the log plot ($K_{MSD}$) was used to assess the directionality of a track, whereby a slope < 1 suggests constrained motion, a slope = 1 suggests Brownian diffusion and a slope > 1 suggests active motion (Figure SI14) (35-37). Considering the mean speed and $K_{MSD}$ together, it was evident that two trajectory types were apparent in the *P .aeruginosa* wildtype population at both the surface and in the bulk (Figure SI15). A cluster of tracks was observed for cells with a mean velocity above 30 µm/s and a $K_{MSD}$ above 1.5, with the remaining trajectories having a mean velocity below 20 µm/s or a $K_{MSD}$ below 1. A similar grouping of trajectories was observed for the *motAB* and *motCD* mutants, although in both cases the separation of the two groups was less evident due to a reduction in the velocity observed for the directionally swimming bacteria (Figure SI15b-c). Trajectories were separated into two classes, the first included bacterial tracks with a high velocity (> 25 µm/s) and a high $K_{MSD}$ (>1.5), whilst the remaining were grouped into the second. Plots of the resulting tracks divided into the two classes are shown in Figure SI13. It was evident that based upon the selection criteria described, the trajectories separated into two clearly distinct cellular phenotypes; in the first, the bacteria moved over large distances in a highly directional manner which have previously been described as *runs,* (Figure 3a) and in the second, frequent reversals in direction were evident, termed *oscillating*. Trajectories that remained at the surface were assigned as *rambling* as opposed to *oscillating*. We assigned runs that remained near the surface (within the focal plane of DIC images) for greater than 1 s as *near surface runs*. We were thus able to automatically assign the trajectory type and exclude the possibility of operator bias. The different trajectory phenotypes were individually assessed to determine frequency, average speed and $K_{MSD}$ (Table 1).

Using the analysis described, the trajectory types of the different mutants were compared at the surface and within the bulk. The bulk bacterial wildtype trajectories were predominantly (64 %) runs, at an average speed of 59 ± 4 µm/s (mean ± standard deviation). In comparison both *motAB* and *motCD* mutants were predominately oscillating (≈54%) and the average run speed was significantly ($p<0.0001$) reduced in both cases to 29 ± 9 µm/s and 45 ± 18 µm/s, respectively (Figure 4a; Table 1). This direct measure of bacterial swimming contrasts with conventional measurements of population swimming speeds in low-viscosity agar whereby under these conditions no change in speed was observed for *P. aeruginosa motAB* and *motCD* mutants (33). In ref 39 different classes of motility were not taken into account. Additionally, increased variance in the speed within a single run trajectory

was also observed for the *motCD* mutants in the bulk (average standard deviation = 32 ± 36 µm/s compared with 18 ± 4 µm/s and 9 ± 1 µm/s for the wildtype and *motAB* strains, respectively. Figure 4a, Table 1). Thus, removal of the *motCD* stator reduced the ability of the bacteria to swim at a constant speed.

The average speed of near surface runs was significantly ($p<0.01$) reduced compared to the average run speed in the bulk for all strains by 7 %, 39 % and 51 % for the wildtype, *motAB* and *motCD* mutants, respectively (Figure 4a-b, Table 1). Thus, strains lacking either of the stators reduced their speed more significantly at the surface than the wildtype strain and, therefore, either reduced their power input or were unable to achieve the same speed for a certain power input within the fluid dynamics experienced at the liquid-solid interface (38, 39). This suggests a key role for the stators in responding to the surface environment and a possible mechanism for surface sensing. The directionality of the run trajectories for all mutants was unaltered either in the bulk or at the surface, with a $K_{MSD}$ of 1.8 to 1.9 observed in all cases (Table 1).

In an oscillating trajectory the bacteria rapidly changed direction (Figure 3c) as a result of the reversal of bacterial flagella rotation. (Figure 3b). Both the wildtype and *motCD* mutant had high oscillating frequencies of 3.1 ± 1.0 Hz and 2.6 ± 0.6 Hz, respectively, whereas the *motAB* mutant exhibited a reduced oscillating frequency of 1.5 ± 1.0 Hz (significant at $p<0.05$). The average instantaneous speed of the oscillating *motAB* mutant was also higher (19 ± 5 µm/s) than the two other strains (≈11 µm/s). As oscillating trajectories were observed for both mutants, either stator appears to be sufficient to support this type of trajectory. However, the altered phenotype of the *motAB* mutant suggests a key role for MotAB in controlling the oscillatory trajectory. The directionality of the oscillating trajectories over a $\delta t$ of 50 to 1000 ms also varied between the two mutants. The $K_{MSD}$ values of 1.2-1.6 were lower than the run trajectories, thus this trajectory type allowed the bacteria to move in a more diffusive manner. A statistically significant increase in $K_{MSD}$ was observed for the *motAB* mutant compared with both the wildtype ($p=0.4$) and *motCD* ($p=0.001$), again suggesting a role for MotAB in regulating the oscillatory trajectory.

At the surface, a statistically significant ($p<0.001$) reduction in average speed was observed between the run and rambling trajectories for the wildtype and *motAB* strains, whereas a significant reduction was not observed for the *motCD* strain (Table 1). For all strains a statistically significant ($p<0.05$) reduction in directionality from a $K_{MSD}$ of 1.8-1.9 to 1.5-1.7 was observed. No significant difference in the $K_{MSD}$ values for the rambling trajectories of the different strains was observed.

In addition, the surface attachment, detachment and reversals for the *mot* mutants was also compared. Within 5 min a larger proportion (72 %) of the wildtype cells were attached to the surface compared with either of the *mot* mutants (≈22 %) (Figure 4c). Of those attached cells, variance was also observed in the ratio of pole-attached to long axis attached cells, with values of 0.42, 2.7 and 1.2 observed for the wildtype, *motAB* and *motCD* mutants respectively (Figure 4c). Switching from long axis to polar attachment has previously been associated with cell surface departure (20). Consistent with this, Figure 4d shows that although

no statistically significant differences were observed between the attachment rates, the detachment rates for both mutants was higher (≈ 2.3 % of attached cells per second) than the wildtype (0.2 % of attached cells per s). Path deviations greater than 120 degrees, classified as reversals, were observed very infrequently for run or rambling tracks. The highest reversal rates were observed for the wildtype bacteria (0.5 ± 0.1 Hz) whilst both *mot* mutants had similar reversal rates of 0.1 ± 0.1 Hz. The reversal rates for all strains increased when the bacteria were involved in near surface runs. Whereas for both wild type and the *motAB* mutant, reversal rates increased 2-fold upon exposure to the surface, the *motCD* mutant increased reversals by 6-fold (Table 1). This result contrasts with reversal rates observed previously for *P. aeruginosa* strain PA14 (33), whereupon the reversal rates observed for the respective *motAB* and *motCD* mutants was 2-3 fold higher than the wildtype. This is likely due to different culture conditions used, specifically the PA14 experiments were conducted using stationary phase bacteria grown in M63 medium supplemented with glucose and with the addition of 3% Ficoll to increase growth medium viscosity and so slow motility to enable imaging. The load responses of *motAB* and *motCD* stators have also been well studied (30) and the order of magnitude differences we observed in the reversal rates of the *motAB* and *motCD* mutants was likely a response to the variation in viscosity. Together these results suggest that the stators play a key role in controlling the interaction of *P. aeruginosa* with a surface, consistent with previous observations (29, 33). A few non-motile cells (<2 %) were observed for all motile strain populations. We also observed flagellar driven spinning for 10-13% of attached cells for all bacterial strains with the exception of the *motABCD* mutant where no spinning was observed, consistent with the flagellar dependent nature of this phenotype (15).

As the motility of log phase bacterial cells was investigated, we observed individual cells in various stages of cell division. To assess the influence of cell division on motility, we compared the trajectories of bacteria undergoing cell division identified via their elongated shapes. The near surface swimming behaviour of dividing cells appeared to be unchanged compared with non-dividing cells (Figure SI16). However, the average speed of swimming, dividing cells was reduced from 40 ± 28 µm/s to 30 ± 17 µm/s, suggesting that during cell division, bacteria swim more slowly, likely as a result of the energetic costs of dividing, competition between the two daughter cell flagella that may not be fully formed, and the increased drag associated with a larger cell body.

To assess the role of the bacterial stators on bacterial surface accumulation, we observed the distributions of the *P. aeruginosa* wildtype and *mot* mutants after 2 h growth. Histograms of the bacterial distribution in the z-axis are shown in Figure SI17 and Figure 5. A higher association of the wildtype and the *motAB* mutant with the two glass surfaces compared to the bulk was observed, both at the top and bottom (Figure 5). For the wildtype bacteria the cell fraction (per µm) was more than 15× greater within 5 µm of the top and bottom surfaces compared with near the surface (5-20 µm) or within the middle of the sample chamber (20-50 µm). Assessment of the cell track classifications reveals that the surface accumulation was due both to near surface swimming and surface attachment. The surface accumulation observed for the *motAB* mutant was significant ($p<0.05$) but not as great as for the wildtype, with the cell fraction per µm at the top and bottom surfaces exceeding the middle of the sample chamber

by 6-8 times. The cell fraction per µm was twice as great for the top and bottom surfaces for the *motAB* mutant compared with the middle of the chamber and for the bottom surface of the *motABCD* mutant. These differences, however, were not statistically significant ($p>0.05$). The minimal surface accumulation for the non-motile *motABCD* mutant was as anticipated given its lack of a flagellum. For the *motCD* mutant, the reduction of surface accumulation for this strain suggests a role for MotCD in surface sensing during the initial attachment stages. Moreover, the similar bulk and surface distributions of the motile *motCD* mutant suggests that the surface accumulation of bacteria cannot be explained by hydrodynamic or steric forces alone but may additionally be actively achieved by altered bacterial behaviour when sensing a surface. No statistically significant differences were observed between the top and bottom surfaces for any of the bacterial strains suggesting that neither gravity nor buoyancy nor chemotaxis/aerotaxis are controlling factors in this experimental set-up ($p>0.06$).

We have developed a multimode 2/3D microscope that combines DIC, DHM, TIRM and TIRF imaging modes to achieve bulk and surface label-free imaging of a motile bacterial population at the single cell level. Bacterial trajectories were assessed using DHM in the bulk and at the surface, categorising different trajectory phenotypes including runs, oscillatory and rambling trajectories within the bacterial cell population at the surface and in the bulk. These could be automatically distinguished by considering the speed and $K_{MSD}$ values for each track together. Combined DHM and TIRM imaging enabled the surface swimming orientation of cells to be determined, revealing that the bulk of cells swam aligned parallel to the surface, with only a small proportion of the population swimming flagellar-pole up or down. High cell density spatial distribution was mapped and quantified by a remote imaging relay used to rapidly acquire DIC z-stacks, from which 3D bacterial distributions could be assessed at an order of magnitude higher of cell concentration than could be achieved using DHM. The utility of this system was used to investigate the role of the *P. aeruginosa* flagella stators *motAB* and *motCD* on cell motility and surface interactions, enabling observations of altered phenotypic behaviour at the single cell level, and suggesting a role for the stators in regulating the interaction of *P. aeruginosa* with a surface. By assessing different trajectory types separately, we identified a significant reduction in run speed for the *mot* mutants. Furthermore, both mutants tended to preferentially adopt the oscillatory trajectory. The altered characteristics of the oscillatory trajectories for the *motAB* mutant compared with the wild type and *motCD* mutant are consistent with a key role for MotAB in regulating this trajectory type. The speed of near surface runs was observed to decrease for all bacterial strains compared to the bulk, however, the greater slowing of the surface speeds observed for the *motAB* and *motCD* mutants demonstrated the key role of the stators for controlling near surface run speed. An increase in the detachment rates of the two mutants compared with the wildtype was also observed, implicating a role for the stators in this key surface event. Moreover, the *motCD* mutant exhibited reduced surface accumulation compared to the wildtype. Together these observations of the contributions of the individual stators to the motile behaviour of individual cells suggest that they play a key but differential role in the initial surface sensing of *P. aeruginosa* prior to any surface association or attachment events. The methods described in the

paper will be of use within the field of single particle tracking and for the comprehensive assessment of the motility behaviours of cell populations at a single cell level within a 3D volume.

## 4. Materials and Methods

### *4.1. Bacterial strains and growth conditions*

*P. aeruginosa* strain PAO1-Washington and the isogenic *motAB*, *motCD* and *motABCD* mutants were each grown at 37°C overnight in LB and diluted to an $OD_{600}$ 0.01 in LB prior to incubating for a further 4 h at 37°C with shaking to reach log phase at an $OD_{600} \approx 1$. Bacterial cultures were diluted to $OD_{600}$ 0.015 in LB before inoculation into analysis chambers. The *mot* mutants were constructed by allelic exchange. Two PCR products amplifying the upstream and the downstream nucleotide regions of *motAB* or *motCD* were generated using the primer pair 1FW/1RW, and 2FW/2RW, respectively (Table SI1). Both PCR products were fused by overlapping PCR to create a deletion in the corresponding gene. The resulting fragment was cloned into the suicide plasmid pME3087 (40). The integration of the suicide plasmid into PAO1 chromosome was carried out by conjugation. Recombinants were selected on tetracycline (125 $\mu g.ml^{-1}$). The second crossing over was carried out by an antibiotic enrichment procedure using Carbenicillin (300 $\mu g.ml^{-1}$) in order to select for the loss of tetracycline resistance. The resulting colonies were screened for the loss of antibiotic resistance by plating on LB supplemented with or without tetracycline. The in-frame deletions were confirmed by PCR and sequence analysis.

For genetic complementation of the in frame deletion mutants the *motAB* and *motCD* genomic regions were PCR-amplified using chromosomal DNA of *P. aeruginosa* as a template and the primer pairs indicated in table SI1. The purified fragments were cloned into the shuttle vector pME6032 (41). The insertions were verified by restriction and sequencing analysis and introduced into the *motAB* and *motCD* mutants by electroporation. The swarming ability of the *mot* mutants was verified by swarming plate assay (data not shown).

### *4.2. Substrate formation*

Two strips of double-sided tape, approximately 2 × 15 × 0.1 mm, were placed on a borosilicate glass coverslip (VWR) in parallel with a gap of ~4 mm. A second glass coverslip was placed on top of the double-sided tape to create a chamber with a floor and ceiling of glass and walls of double-sided tape. The second coverslip was rotated 45° to allow ease of loading the channel with growth medium. After inoculation with bacteria, the two ends of the chamber were sealed using silicone free grease (Apiezon).

### *4.3. Microscopy*

Imaging was achieved using a bespoke multimode microscope (Cairn Ltd.). Samples were analysed at 37°C using a Nikon Eclipse Ti inverted microscope using a 60×, NA=1.49, WD=0.13 mm oil objective. The microscope was fitted with an environmental chamber (Okolab) to regulate temperature, relative humidity and $CO_2$. Images were acquired using an Orca-Flash 4.0 digital CMOS camera (Hamamatsu) at a typical acquisition rate of 41.6 Hz. DIC imaging was achieved using a single channel white MonoLED (Cairns) light source. A polariser was inserted above the condenser, and Wollaston prisms were inserted between the condenser and polariser and below the objective. DHM imaging was acquired using a 685 nm LX laser (Obis). TIRM was conducted using a Obis 488 nm LX laser (Cairn) controlled using an illumination system (iLas2). The sample was illuminated through the objective by use of a 50 % mirror, controlled to achieve total internal reflectance by irradiating the sample at an incidence angle ($\theta$) greater than the critical angle ($\theta_c$) given by equation 1, where $n_1$ is the refractive index of the incident medium and $n_2$ is the refractive index of the transmission medium.

$$\sin(\theta_c) = \frac{n_2}{n_1} \quad (1)$$

Bacterial imaging was achieved through the local change in refractive index and $\theta_c$ induced upon bacteria entering the evanescent field caused by the TIR. The penetration depth ($d$) of the evanescent field was determined using equation 2, where $\lambda$ is the wavelength of the light = 488 nm, and tuned to 200 nm.

$$d = \frac{\lambda}{4\pi}[n_1^2 sin^2(\theta) - n_2^2]^{-1/2} \quad (2)$$

A total of 5 biological repeats for each mutant was prepared and imaged by interlaced capture of DHM with either DIC or TIRM. Each image sequence consisted of 2000 frames (1000 frames for each acquisition mode) for a total duration of 48 s.

Z-stack images were acquired using a bespoke remote focussing assembly as described previously (42).

To observe flagella orientation during reversals, PAO1 was fluorescently stained using Alexa Fluor carboxylic acid succinimidyl esters (Alexa Fluor 488, ThermoFisher) as described previously (Friedlander et al. 2013; Turner, Ryu, and Berg 2000). PAO1 cells were grown overnight in LB medium at 37 °C and 200 rpm. They were resuspended and diluted in fresh LB medium at $OD_{600}$ = 0.01. When cells reached exponential phase, they were centrifuged at 2,000 x g for 10 min and growth medium removed. The pellet was resuspended gently in a wash buffer of 10−2 M $KPO_4$, 6.7 x 10−2 M NaCl, 10−4 M EDTA, pH-adjusted to 7.0 with HCl, and then centrifuged to pellet the cells. After two additional rinses, cells were incubated with 0.5 mg/mL Alexa Fluor carboxylic acid succinimidyl ester for 1 h at room temperature, gently rocking. Residual dye was removed after washing twice and then the cells were resuspended in PBS for imaging.

### *4.4. Image processing*

After acquisition, holograms were processed using a bespoke Matlab script (ImageProcess). Image intensity across a stack was normalised, then the median image over the stack was subtracted to remove background signal, also including attached cells. DHM image output sequences were reconstructed using a bespoke Python algorithm (43) making use of Rayleigh-Sommerfeld formalism to determine bacterial X-Y-Z coordinates. Bacterial trajectories were determined using a bespoke Matlab script (DHMTracking). To exclude noise a voxel limit was set and applied to each image such that a similar number of objects were identified in each frame. Visual inspection of interferogram image sequences enabled an estimate of the number of bacteria per frame to ensure the voxel limit was set so as not to exclude bacterial cells. Bacterial trajectories were determined using the bespoke Matlab script (tracking). Objects were matched with their nearest neighbour within the next frame, applying a distance limit based upon the maximum speed of bacteria (100 µm/s). The script looked up to 4 frames ahead for a matching object. All tracks were also visually inspected using a bespoke Matlab script (Graphing) to ensure trajectories skipping more than 4 frames could be joined. All Matlab scripts are published as a part of the Supplementary information.

The MSD of tracks were calculated using a bespoke Matlab script (ROC_MSD). Mean squared displacement (MSD) was calculated according to equation 3, where $\vec{x}(t_j) = \vec{R}_j$ and was the vector of the $j^{th}$ point on the trajectory and the angled brackets indicates an all measurements for a given time $t_i$ (44).

$$\Delta x^2(t) = \langle (\vec{x}(t_{i+1}) - \vec{x}(t_i))^2 \rangle \quad (3)$$

DIC images and Z-stacks were processed using a bespoke Matlab script (StackMaster). Each image was flattened by a line-by-line polynomial fit. A threshold was then applied to binarise the image to segment pixels with bacteria. Threshold was set as $signal^2:noise^2 > 10$. The square of the signal was measured so as to identify both bright and dark regions associated with the DIC image. Objects less than 20 pixels were excluded as noise. Holes within objects were filled using the Matlab function 'imfill'. Bright and dark regions were paired based upon proximity and a common directional vector between objects within the same frame. The centre of mass of objects was calculated giving equal weighting to bright and dark regions. The length and width of the smallest rectangle around an object and the orientation of the bacteria was determined using a bespoke Matlab script (ParticleAnalysisDIC). For DIC Z-stacks, objects on consecutive frames were analysed to identify overlapping pixels considering the X-Y dimensions. If common pixels were identified objects were groups to form a single object and the centre of mass was determined for this object based upon the combined pixels (Figure SI6) using a bespoke Matlab script (DICZStack_ImageProcessing). Bacterial trajectories were determined as described for DHM data.

TIRM images were processed using ImageJ 1.50b. When processing interlaced DHM and TIRM images the centre of mass of moving cells as determined by DHM was shifted to the average position between two adjacent frames to account for the 20 ms offset between the capture of TIRM and DHM images.

## Figures

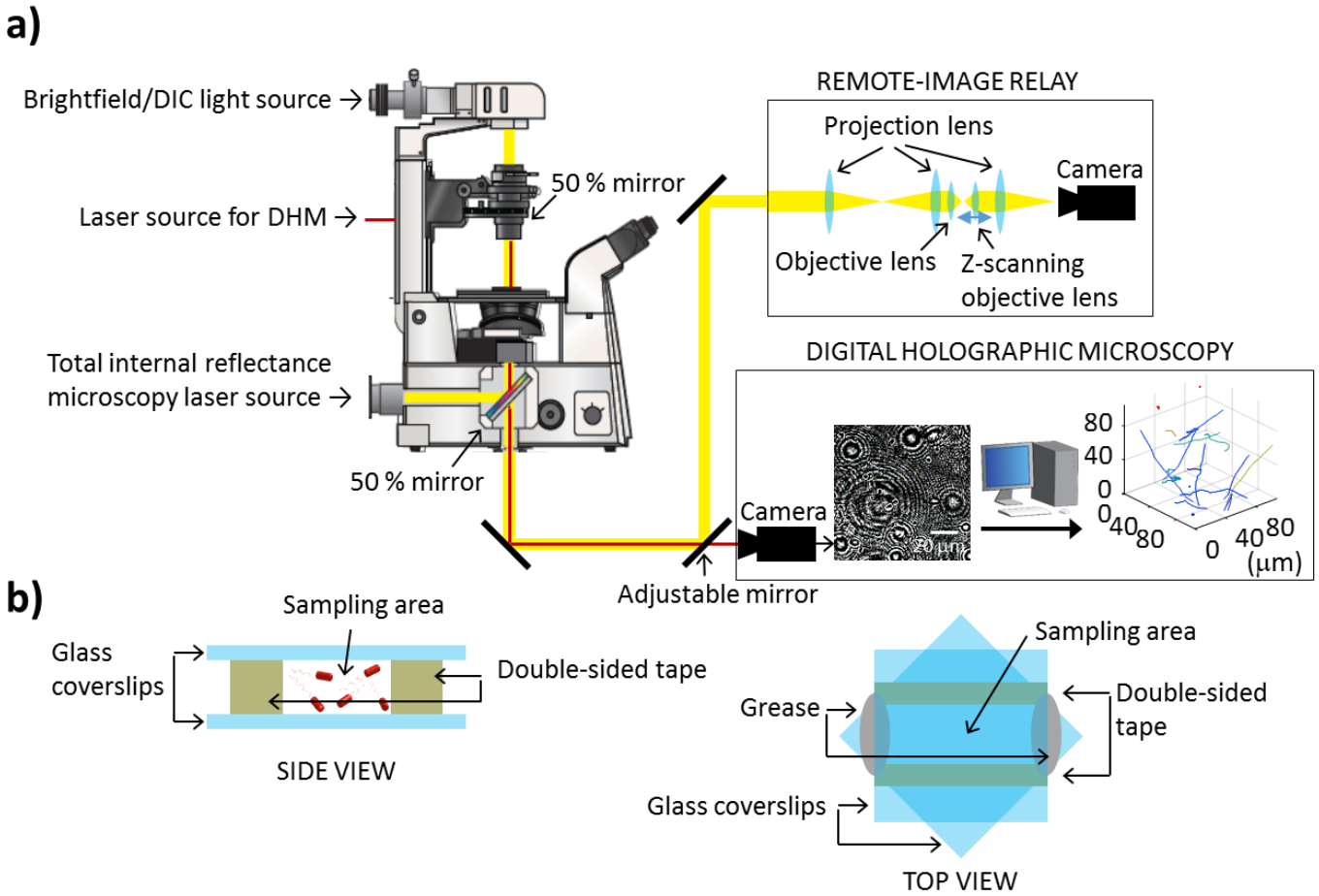


Figure 1. a) Schematic of the multimode 2/3D microscope used in this study including the optical ensemble for the remote-image relay. The Remote Image Relay allows scanning of the focal plane to reconstruct z-stacks without disturbing the sample. The microscope is also equipped with lasers to enable digital holographic microscopy (DHM) and total internal reflectance microscopy (TIRM). b) Schematic of the sample format used in this study including a side and top view. The z-height of the sample volume (distance between glass slides) was 100 µm. The typical separation between the two strips of double-sided tape was 5 mm. The two coverslips were orientated at 45° to each other to enable the easy sealing of the channel ends with hydrocarbon grease.

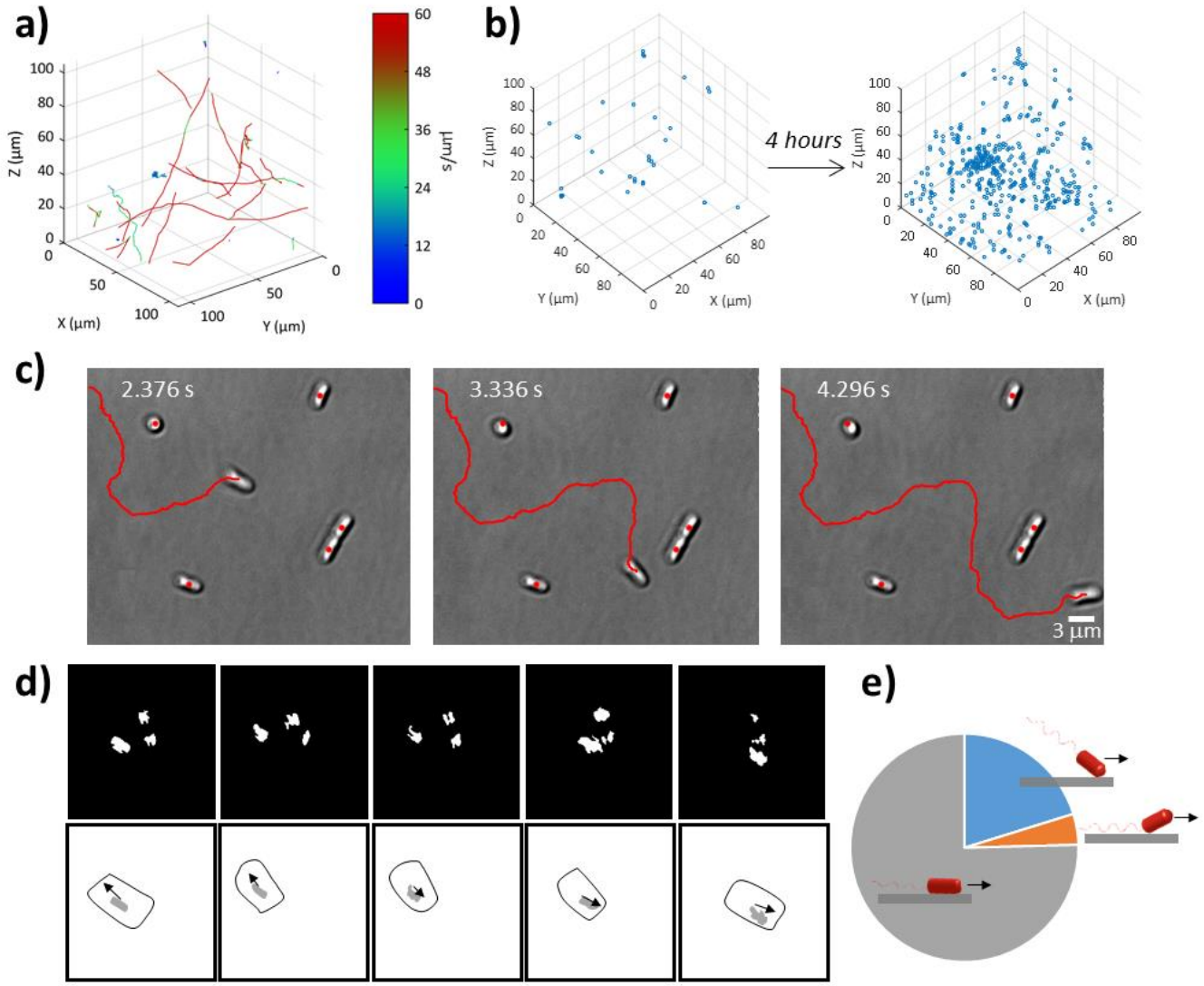


Figure 2. 2D and 3D imaging of *P. aeruginosa* wild-type bacterial trajectories. (**a**) **DHM** isometric view of bacterial trajectories for one continuous 20 s acquisition at 41.7 Hz. Trajectories have been coloured by the instantaneous speed of the track according to the intensity scale provided. (**b**) **DIC Z-stack** of instantaneous bacterial 3D positions at seeding conditions and after 4 h incubation acquired using the remote image relay illustrating the high cell density that can be located and tracked using this method. (**c**) DIC image sequence of *P. aeruginosa* cells swimming at the glass surface with 960 ms between images shown (complete image sequence is available in the supplementary information Figure SI1). The trajectory is shown in red. Of note is the change in bacterial orientation that matched the change in direction during the journey. The image sequence also contains examples of long-axis (side) and polar (end) attached cells. The centre of mass of each cell at time = 2.376 s is indicated as a red dot in each frame, the centre of mass of side attached cells remained unchanged whereas a change in centre of mass location was observed for the end attached cell. (**d**) TIRM image sequence showing a direction reversal. Time interval of 40 ms between each displayed frame. The complete image sequence is available in the supplementary information (Figure SI2). Images shown have been binarised and objects with an area less than 100 pixels, deemed to be noise, were removed. To aid in visualisation the outline (determined from DHM) of the moving cell is shown beneath the corresponding composite image along with the smoothed area of the cell imaged by TIRM (grey). The displacement vector of the centre of mass of the cell (determined from DHM) is also shown as an arrow. **e**) Distribution of the position of the centre of mass of the TIRM spot within the cell body for 9 cells observed to be swimming parallel to the surface over a total of 183 frames, either at the front pole (blue), middle (grey) or rear pole (orange) of the cell (shown schematically where the arrows indicate the direction of travel of the bacterium). The front and rear of the cell were determined from the direction the bacterial cell was travelling subsequent to an image being taken. The TIRM spot was assigned as middle if it was less than 1 micron from the centre of mass of the cell as determined by DHM.

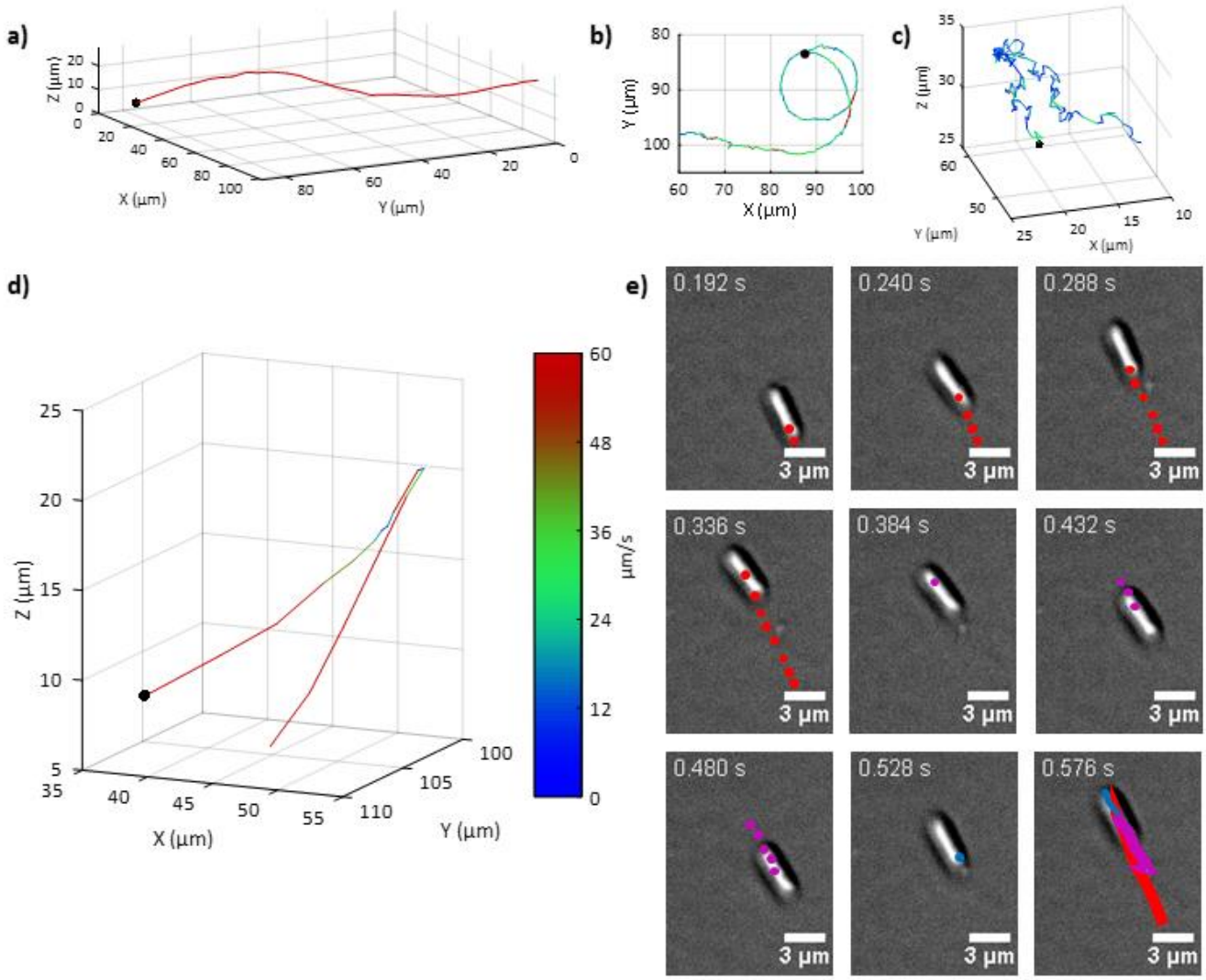


Figure 3. Characterisation of bacterial swimming trajectories. Imaging of bacterial direction change, both in the bulk and at the surface of a material. (a-c) A number of different trajectory phenotypes were observed including: (a) **run trajectory** characterised by relatively long stretches of uninterrupted straight motion (track duration = 1.536 s), (b) near surface run with increased curvature (track duration = 4.872 s) and, (c) **oscillating trajectories** characterised by frequent changes in direction (track duration = 9.840 s). A black dot marks the beginning of each track. The track is coloured by the instantaneous speed according to the intensity scale shown in (d). (d) Example of bacterial reversal directional change as observed by DHM within the bulk. The start of the trajectory is indicated by a black dot. The track is coloured by the instantaneous speed according to the intensity scale. Track duration = 0.720 s. (e) Image sequence of two reversal events measured at the surface by DIC. The time between images is 48 ms. The centre of mass of the cell from previous frames is shown as coloured dots. The trajectory consists of the sequence forward-reverse-forward, and each segment has been coloured red-magenta-blue, respectively. The entire trajectory is shown as coloured lines on the final image shown. The two reversal events were observed around time points 0.336 s and 0.480 s whereupon the cell was observed to pause for a frame such that the centre of mass of the cell remained unchanged between two frames.

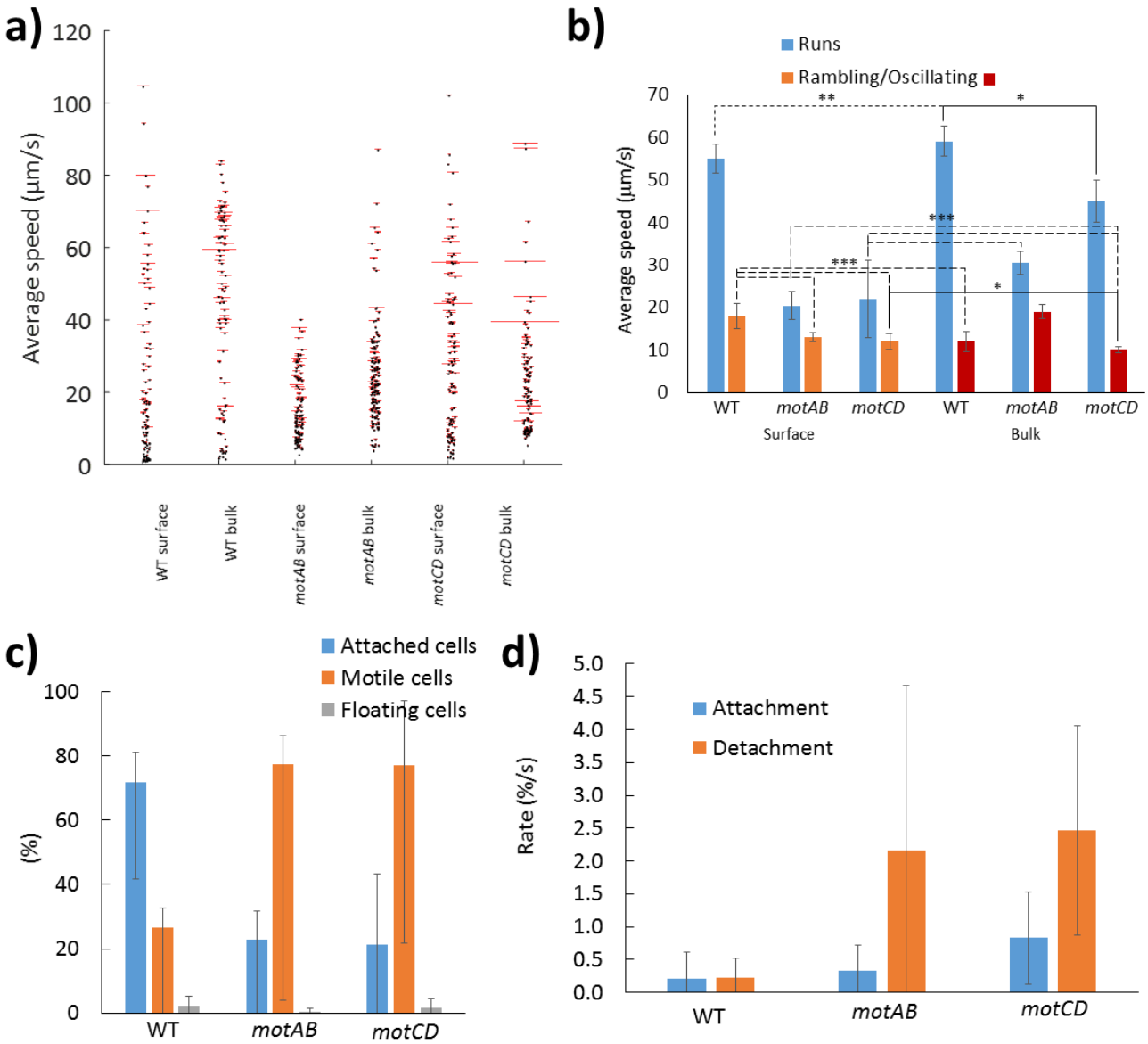


Figure 4. Comparison of the surface (DIC) and bulk (DHM) motility of *P. aeruginosa* wildtype and *motAB* and *motCD* mutants **a)** Comparison of the bulk and surface runs for speed. Each black dot is the measured average speed for a trajectory whilst the length of the associated red line is proportional to the standard deviation of the speed measured between frames over the trajectory length. **b)** Comparison of the average speed measured for the run (■), oscillating (■) and rambling (■) trajectories of *P. aeruginosa* wildtype and *motAB* and *motCD* mutants. The mean value is taken by averaging the speeds across 5 biological replicates. Error bars equal ± 95% confidence limits. Statistically significant differences of $p<0.05$ (*, solid line), $p<0.01$ (**, dotted line) and $p<0.001$ (***, dashed line) are shown. No difference or $p<0.0001$ differences are not shown. **c)** Assessment of the attachment profile for each bacterial strain, reporting the total proportion of attached cells (■) and the proportion of attached cells either polar (■) or long-axis (■) attached**. d)** Attachment (■) and detachment (■) rates measured at the surface and reported as the % of non-attached cells attaching per s or the % of attached cells detaching per s. Error bars equal ± 1 standard deviation unit, N = 5.

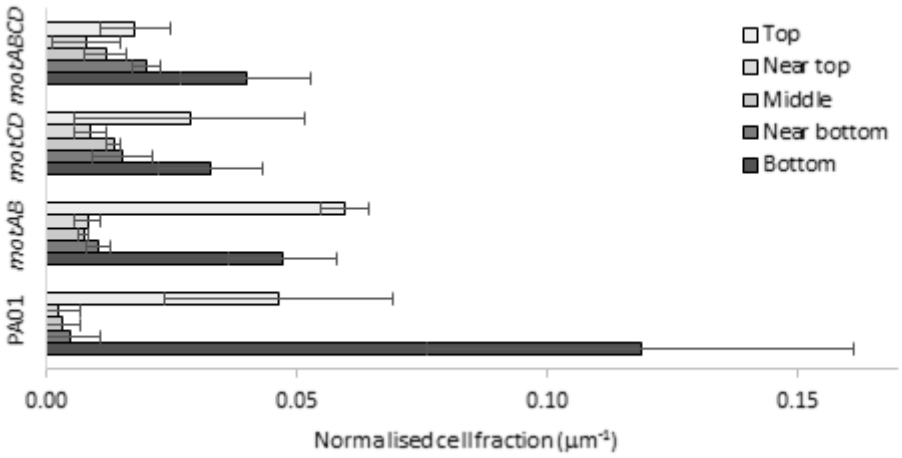


Figure 5. The normalised cell fraction (normalised to unit length in z axis) observed at varied z-regions within the sample chamber. Un-normalised data shown in Figure SI17. Regions studied were bottom and top areas equal to 0-5 μm from the surface, near top and bottom equal to 5-20 μm from the surface, and the middle region. The average number of bacteria measured within the volume for each strain after the 5 min was wildtype = 54, *motAB* = 21, *motCD* = 27, and *motABCD* = 15. Error bars equal ± 1 standard deviation unit from 3 biological replicates. Area imaged was 120 × 120 μm.

Table 1. Summary of quantification of surface tracks including both surface and bulk measurements. Speeds presented are the average speeds measured over frame intervals of 24 ms. Speed variance is the average standard deviation for the instantaneous speeds measured for an entire trajectory. The ranges quoted are one standard deviation of such measurements for each cell; WT, wildtype

| | ***Surface*** | | | ***Bulk*** | | |
|---|---|---|---|---|---|---|
| | WT | *motAB* | *motCD* | WT | *motAB* | *motCD* |
| **Classification of cells** | | | | | | |
| Number of tracks | 150 | 138 | 142 | 71 | 154 | 97 |
| Motile (%) | 27 ± 6 | 77 ± 9 | 77 ± 20 | 97 ± 7 | 97 ± 3 | 100 ± 0 |
| -runs (% of motile cells) | 51 ± 6 | 10 ± 2 | 25 ± 28 | 64 ± 31 | 45 ± 10 | 46 ± 34 |
| -near surface runs (% of motile cells) | 18 ± 9 | 54 ± 4 | 43 ± 16 | | | |
| -rambling (*surface*) / oscillating (*bulk*) (% of motile cells) | 31 ± 12 | 36 ± 5 | 32 ± 21 | 36 ± 31 | 55 ± 10 | 54 ± 34 |
| Attached (%) | 72 ± 9 | 23 ± 9 | 21 ± 22 | | | |
| -polar attached (% of attached cells) | 30 ± 14 | 73 ± 26 | 55 ± 31 | | | |
| -long-axis attached (% of attached cells) | 70 ± 14 | 27 ± 26 | 45 ± 31 | | | |
| Floating (%) | 2 ± 3 | 0 ± 1 | 2 ± 3 | 3 ± 7 | 3 ± 3 | 0 ± 0 |
| **Direction change analysis** | | | | | | |
| Frequency of reversal events for cell runs (Hz) | 0.9 ± 0.4 | 0.2 ± 0.0 | 0.6 ± 0.3 | 0.5 ± 0.1 | 0.1 ± 0.0 | 0.1 ± 0.1 |
| Oscillating frequency | | | | 3.1 ± 1.0 | 1.5 ± 1.0 | 2.6 ± 0.6 |
| Rambling frequency (Hz) | 3.2 ± 2.1 | 2.9 ± 1.5 | 6.1 ± 0.7 | | | |
| **Arrival and departure events from the surface** | | | | | | |
| Attachment rate (% of non-attached cells per second) | 0.2 ± 0.4 | 0.3 ± 0.4 | 0.8 ± 0.7 | | | |
| Detachment rate (% of attached cells per second) | 0.2 ± 0.3 | 2.2 ± 2.5 | 2.5 ± 1.6 | | | |
| **Motility characterisation** | | | | | | |
| | ***Surface run*** | | | ***Run*** | | |
| Speed (μm/s) | 55 ± 7 | 18 ± 5 | 22 ± 21 | 59 ± 4 | 29 ± 9 | 45 ± 18 |
| Speed variance | 23 ± 6 | 10 ± 6 | 16 ± 12 | 18 ± 4 | 9 ± 1 | 32 ± 36 |
| $K_{MSD}$ ($\mu m^2/s$) | 1.9 ± 0.2 | 1.9 ± 0.3 | 1.8 ± 0.2 | 1.9 ± 0.3 | 1.8 ± 0.4 | 1.9 ± 0.2 |
| | ***Rambling*** | | | ***Oscillating*** | | |
| Speed (μm/s) | 18 ± 8 | 13 ± 4 | 12 ± 4 | 12 ± 5 | 19 ± 5 | 10 ± 2 |
| Speed variance | 11 ± 5 | 8 ± 4 | 11 ± 3 | 11 ± 8 | 9 ± 2 | 5 ± 1.3 |
| $K_{MSD}$ ($\mu m^2/s$) | 1.7 ± 0.3 | 1.7 ± 0.4 | 1.5 ± 0.4 | 1.2 ± 1 | 1.6 ± 0.4 | 1.3 ± 0.3 |

## 5. References


1. Wood TK, Gonzalez Barrios AF, Herzberg M, Lee J. Motility influences biofilm architecture in Escherichia coli. Appl Microbiol Biotechnol. 2006;72(2):361-7.
2. Berg HC, Brown DA. Chemotaxis in Escherichia coli analysed by three-dimensional tracking. Nature. 1972;239(5374):500-4.
3. Xie L, Altindal T, Chattopadhyay S, Wu XL. From the Cover: Bacterial flagellum as a propeller and as a rudder for efficient chemotaxis. Proc Natl Acad Sci U S A. 2011;108(6):2246-51.
4. O'Toole GA, Wong GCL. Sensational biofilms: surface sensing in bacteria. Current Opinion in Microbiology. 2016;30:139-46.
5. Shen H, Tauzin LJ, Baiyasi R, Wang WX, Moringo N, Shuang B, et al. Single Particle Tracking: From Theory to Biophysical Applications. Chemical Reviews. 2017;117(11):7331-76.
6. Frymier PD, Ford RM, Berg HC, Cummings PT. Three-dimensional tracking of motile bacteria near a solid planar surface. Proceedings of the National Academy of Sciences. 1995;92(13):6195-9.
7. Rabut G, Ellenberg J. Automatic real-time three-dimensional cell tracking by fluorescence microscopy. Journal of Microscopy-Oxford. 2004;216:131-7.
8. Wu MM, Roberts JW, Buckley M. Three-dimensional fluorescent particle tracking at micron-scale using a single camera. Experiments in Fluids. 2005;38(4):461-5.
9. Li GL, Bensson J, Nisimova L, Munger D, Mahautmr P, Tang JX, et al. Accumulation of swimming bacteria near a solid surface. Physical Review E. 2011;84(4).
10. Taute KM, Gude S, Tans SJ, Shimizu TS. High-throughput 3D tracking of bacteria on a standard phase contrast microscope. Nature Communications. 2015;6.
11. Vater SM, Weisse S, Maleschlijski S, Lotz C, Koschitzki F, Schwartz T, et al. Swimming Behavior of Pseudomonas aeruginosa Studied by Holographic 3D Tracking. Plos One. 2014;9(1).
12. Lee SJ, Go T, Byeon H. Three-dimensional swimming motility of microorganism in the near-wall region. Experiments in Fluids. 2016;57(2).
13. Taylor BL, Koshland Jr. DE. Reversal of Flagellar Rotation in Monotrichous and Peritrichous Bacteria: Generation of Changes in Direction. J Bacteriol. 1974;119(2):640-2.
14. Bianchi S, Saglimbeni F, Di Leonardo R. Holographic Imaging Reveals the Mechanism of Wall Entrapment in Swimming Bacteria. Physical Review X. 2017;7(1).
15. Conrad JCCJC, Gibiansky ML, Jin F, Gordon VD, Motto DA, Mathewson MA, et al. Flagella and Pili-Mediated Near-Surface Single-Cell Motility Mechanisms in P. aeruginosa. Biophysical Journal. 2011;100(7):1608-16.
16. Kearns DB. A field guide to bacterial swarming motility. Nature Reviews Microbiology. 2010;8:634-44.
17. Berg HC, Turner L. Cells of Escherichia-coli swim either end forward. Proceedings of the National Academy of Sciences of the United States of America. 1995;92(2):477-9.
18. Berke AP, Turner L, Berg HC, Lauga E. Hydrodynamic attraction of swimming microorganisms by surfaces. Physical Review Letters. 2008;101(3).
19. Shum H, Gaffney EA, Smith DJ. Modelling bacterial behaviour close to a no-slip plane boundary: the influence of bacterial geometry. Proceedings of the Royal Society a-Mathematical Physical and Engineering Sciences. 2010;466(2118):1725-48.
20. Conrad JC. Physics of bacterial near-surface motility using flagella and type IV pili: implications for biofilm formation. Research in Microbiology. 2012;163(9-10):619-29.
21. Bartholomew JW. Flagellation of Certain Species of Pseudomonas as seen with the electron microscope. Journal of General Microbiology. 1949;3(3):340-6.
22. Tailleur J, Cates ME. Statistical mechanics of interacting run-and-tumble bacteria. Physical Review Letters. 2008;100(21).
23. Hintsche M, Waljor V, Grossmann R, Kuehn MJ, Thormann KM, Peruani F, et al. A polar bundle of flagella can drive bacterial swimming by pushing, pulling, or coiling around the cell body. Scientific Reports. 2017;7.
24. Ping LY. Cell orientation of swimming bacteria: From theoretical simulation to experimental evaluation. Science China-Life Sciences. 2012;55(3):202-9.
25. Ping LY, Birkenbeil J, Monajembashi S. Swimming behavior of the monotrichous bacterium Pseudomonas fluorescens SBW25. Fems Microbiology Ecology. 2013;86(1):36-44.
26. Costerton JW, Stewart PS, Greenberg EP. Bacterial biofilms: A common cause of persistent infections. Science. 1999;284(5418):1318-22.
27. Potron A, Poirel L, Nordmann P. Emerging broad-spectrum resistance in Pseudomonas aeruginosa and Acinetobacter baumannii: Mechanisms and epidemiology. International Journal of Antimicrobial Agents. 2015;45(6):568-85.
28. Hook AL, Chang C, Yang J, Luckett J, Cockrayne A, Atkinson S, et al. Combinatorial discovery of polymers resistant to bacterial attachment. Nature Biotechnology. 2012;30(9):868-75.
29. Sauer K, Camper AK, Ehrlich GD, Costerton JW, Davies DG. Pseudomonas aeruginosa displays multiple phenotypes during development as a biofilm. J Bacteriol. 2002;184(4):1140-54.
30. Baker AE, O'Toole GA. Bacteria, Rev Your Engines: Stator Dynamics Regulate Flagellar Motility. J Bacteriol. 2017;199(12).
31. Doyle TB, Hawkins AC, McCarter LL. The complex flagellar torque generator of Pseudomonas aeruginosa. J Bacteriol. 2004;186(19):6341-50.
32. Kuchma SL, Delalez NJ, Filkins LM, Snavely EA, Armitage JP, O'Toole GA. Cyclic Di-GMP-Mediated Repression of Swarming Motility by Pseudomonas aeruginosa PA14 Requires the MotAB Stator. J Bacteriol. 2015;197(3):420-30.

33. Toutain CM, Caizza NC, Zegans ME, O'Toole GA. Roles for flagellar stators in biofilm formation by Pseudomonas aeruginosa. Research in Microbiology. 2007;158(5):471-7.
34. Toutain CM, Zegans ME, O'Toole GA. Evidence for two flagellar stators and their role in the motility of Pseudomonas aeruginosa. J Bacteriol. 2005;187(2):771-7.
35. Theves M, Taktikos J, Zaburdaev V, Stark H, Beta C. A Bacterial Swimmer with Two Alternating Speeds of Propagation. Biophysical Journal. 2013;105(8):1915-24.
36. Wu XL, Libchaber A. Particle diffusion in a quasi-two-dimensional bacterial bath. Physical Review Letters. 2000;84(13):3017-20.
37. Bouchaud JP, Georges A. Anomalous diffution on disordered media - statistical mechanisms, models and physical applications. Physics Reports-Review Section of Physics Letters. 1990;195(4-5):127-293.
38. Vanloosdrecht MCM, Lyklema J, Norde W, Zehnder AJB. Influence of interfaces on microbial activity. Microbiological Reviews. 1990;54(1):75-87.
39. Zhu YX, Granick S. Viscosity of interfacial water. Physical Review Letters. 2001;87(9).
40. Voisard C, Bull CT, Keel C, Laville J, Maurhofer M, Schnider U, et al. Biocontrol of root diseases by Pseudomonas fluorescens CHA0: current concepts and experimental approaches. Ogara F, Dowling DN, Boesten B, editors1994. 67-89 p.
41. Heeb S, Itoh Y, Nishijyo T, Schnider U, Keel C, Wade J, et al. Small, stable shuttle vectors based on the minimal pVS1 replicon for use in gram-negative, plant-associated bacteria. Molecular Plant-Microbe Interactions. 2000;13(2):232-7.
42. Botcherby EJ, Juskaitis R, Booth MJ, Wilson T. An optical technique for remote focusing in microscopy. Optics Communications. 2008;281(4):880-7.
43. Flewellen JL, Zaid IM, Berry RM. A multi-mode digital holographic microscope. Rev Sci Instr. 2018;In press.
44. Utada AS, Bennett RR, Fong JCN, Gibiansky ML, Yildiz FH, Golestanian R, et al. Vibrio cholerae use pili and flagella synergistically to effect motility switching and conditional surface attachment. Nature Communications. 2014;5.

# Simultaneous tracking of cell motility in liquid and at the solid-liquid interface

## Supplementary information

Andrew L. Hook, James L. Flewellen, Irwin M. Zaid, Richard M. Berry, Jean-Frédéric Dubern, Alessandro Carabelli,

Ricky Wildman, Noah Russell, Paul Williams, Morgan R. Alexander

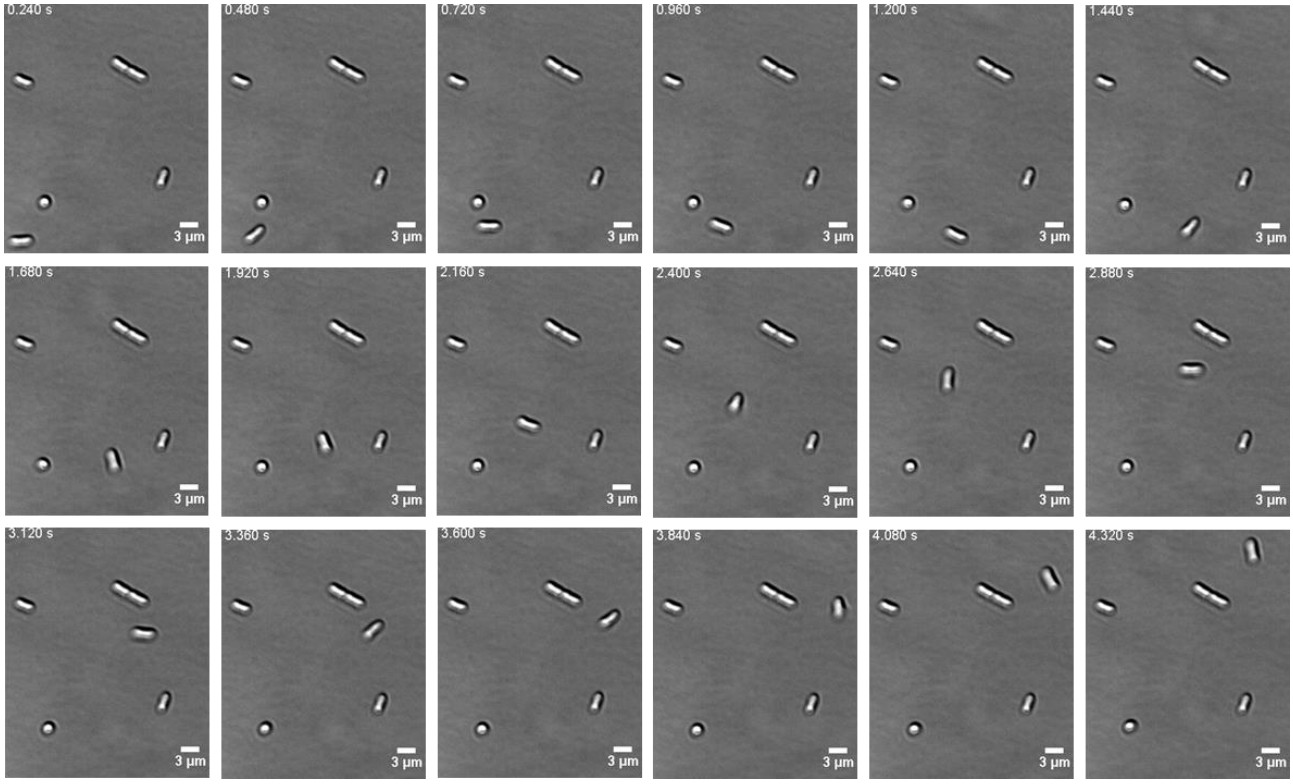


Figure SI1. DIC image sequence of *P. aeruginosa* wild-type cells at a glass surface. Image sequence provides examples of surface rambling, pole and long-axis attached cells. Image interval is 240 ms. See also supplementary video 1.

**a)**

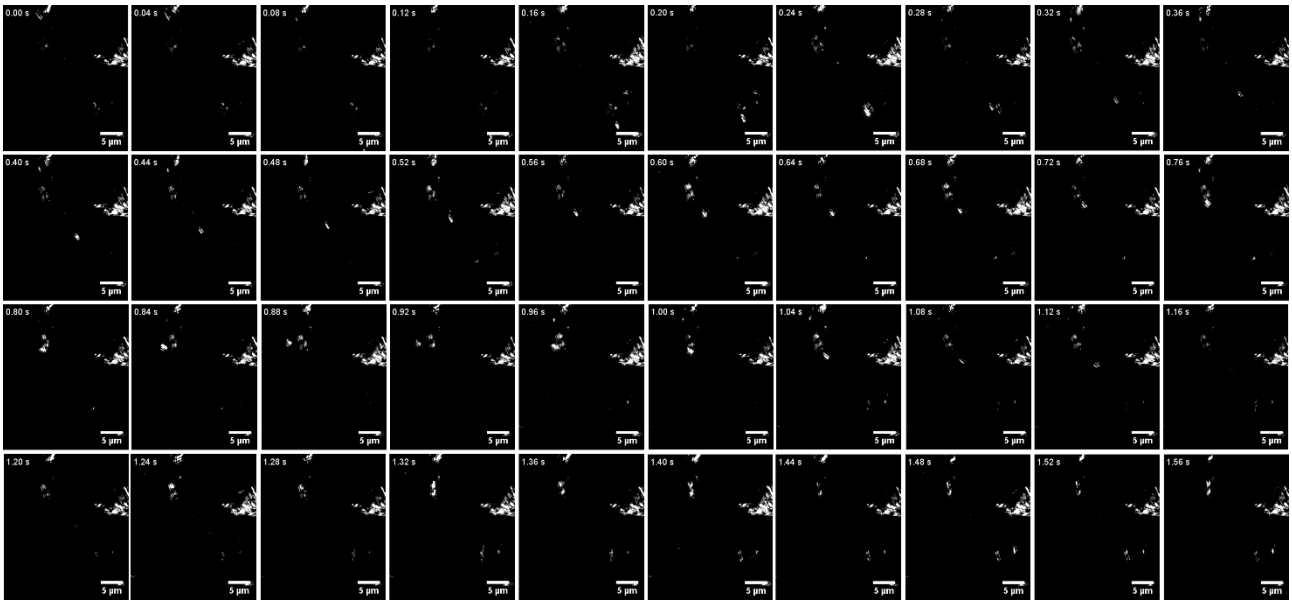

**b)**

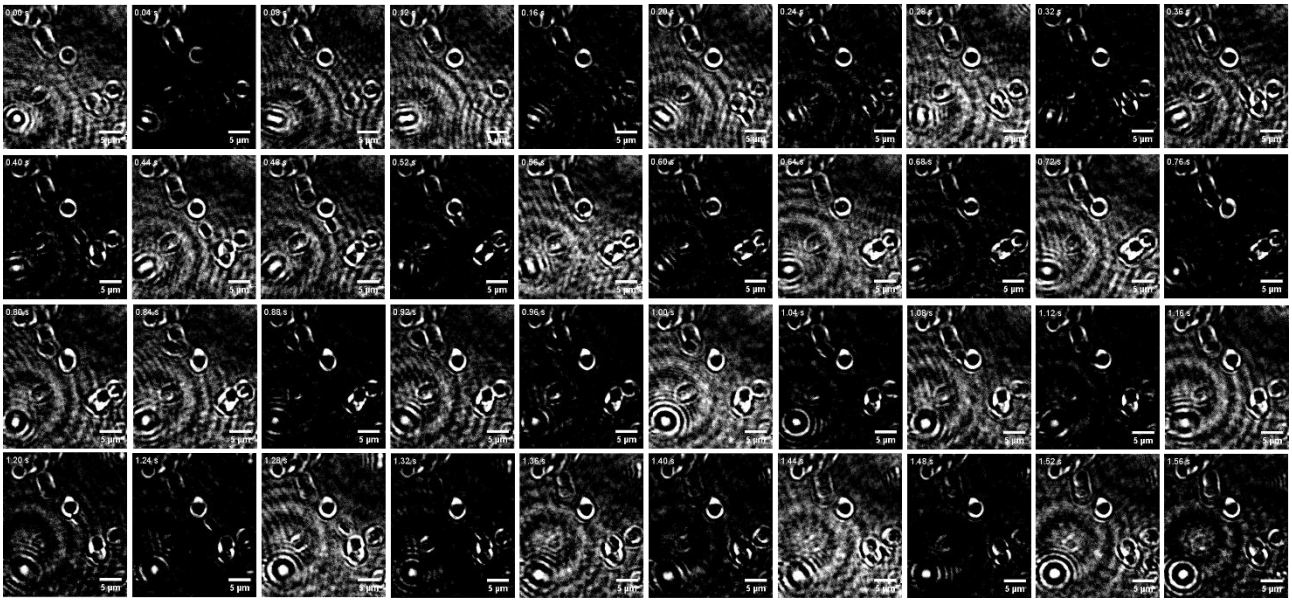

Figure SI2. Image sequence of interlaced TIRM/DHM imaging of *P. aeruginosa* wild-type at a glass interface. Images were taken at intervals of 40 ms. a) TIRM images, b) DHM images. TIRM images acquired 20 ms after the time indicated on the image. See also supplenetary video 2.

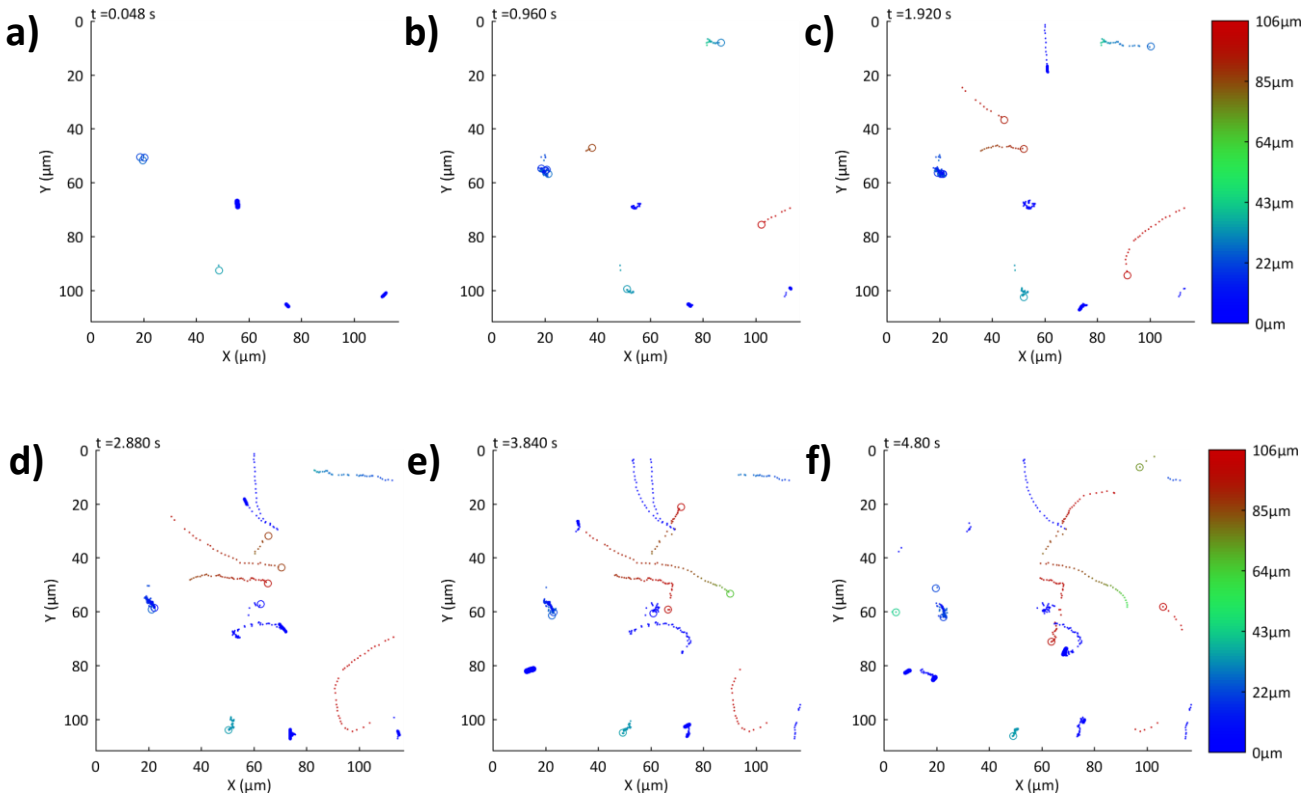


Figure SI3. (**a-f**) Image sequence showing tracking of *P. aeruginosa* wild-type by interlaced DIC and DHM. Time indicated is the position of bacterial cells when the DHM image was acquired; DIC image acquired 24 ms after time indicated. Z-position of bacteria indicated by the colour of the marker according to the intensity scale on the right. Where the object is observed at the surface, the shape and orientation of the object is shown, otherwise the position of each bacterium is indicated as an open circle. The equivalent DIC and DHM images from the 6 images shown are provided in the supplementary information (Figure SI18). Images taken at times (**a**) 0.048 s, (**b**) 0.960 s, (**c**) 1.920 s, (**d**) 2.880 s, (**e**) 3.840 s and (**f**) 4.800 s. Trailing dots represent object position in the previous frame, time between frames = 48 ms. Trailing tracks have been limited in length to 2.4 s.

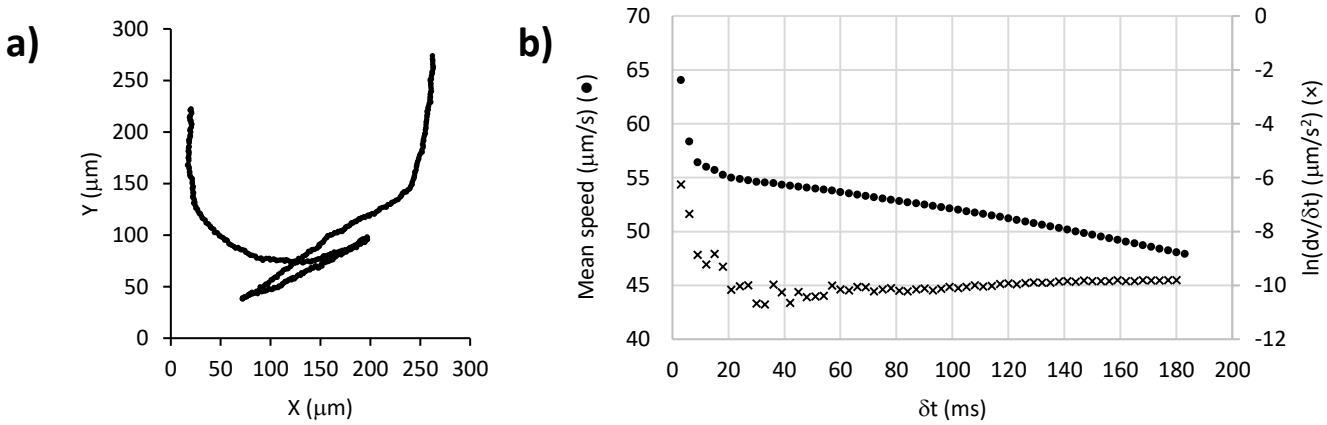


Figure SI4. **a**) X-Y coordinates of a bacterial trajectory taken with DIC. **b**) The mean speed measured for a bacterial trajectory at high frame rate (333 Hz) when the speed was measured between different time intervals. The higher mean speed measured at shorter time intervals suggest that the bacteria experience fluctuating motion over a small time scale. The mean speed was observed to decrease to a minimum in the differential $dv/\delta t$ within the region of 20-60 ms. Above 40 ms a further decrease in the measured mean speed was observed suggesting that at these time intervals the measurements were undersampled with respect to the directional motion of the bacteria. Assuming the bacteria were a sphere of diameter = 3 µm, mass = $6.25 \times 10^{-13}$ kg and a media viscosity of 0.6913 mPa.s at 37 $^{o}$C the Brownian motion frequency as determined by Stokes law = $3.12 \times 10^{4}$ Hz, suggesting that Brownian motion is undersampled at all imaging frequencies. See also supplementary video 3 for full image sequence.

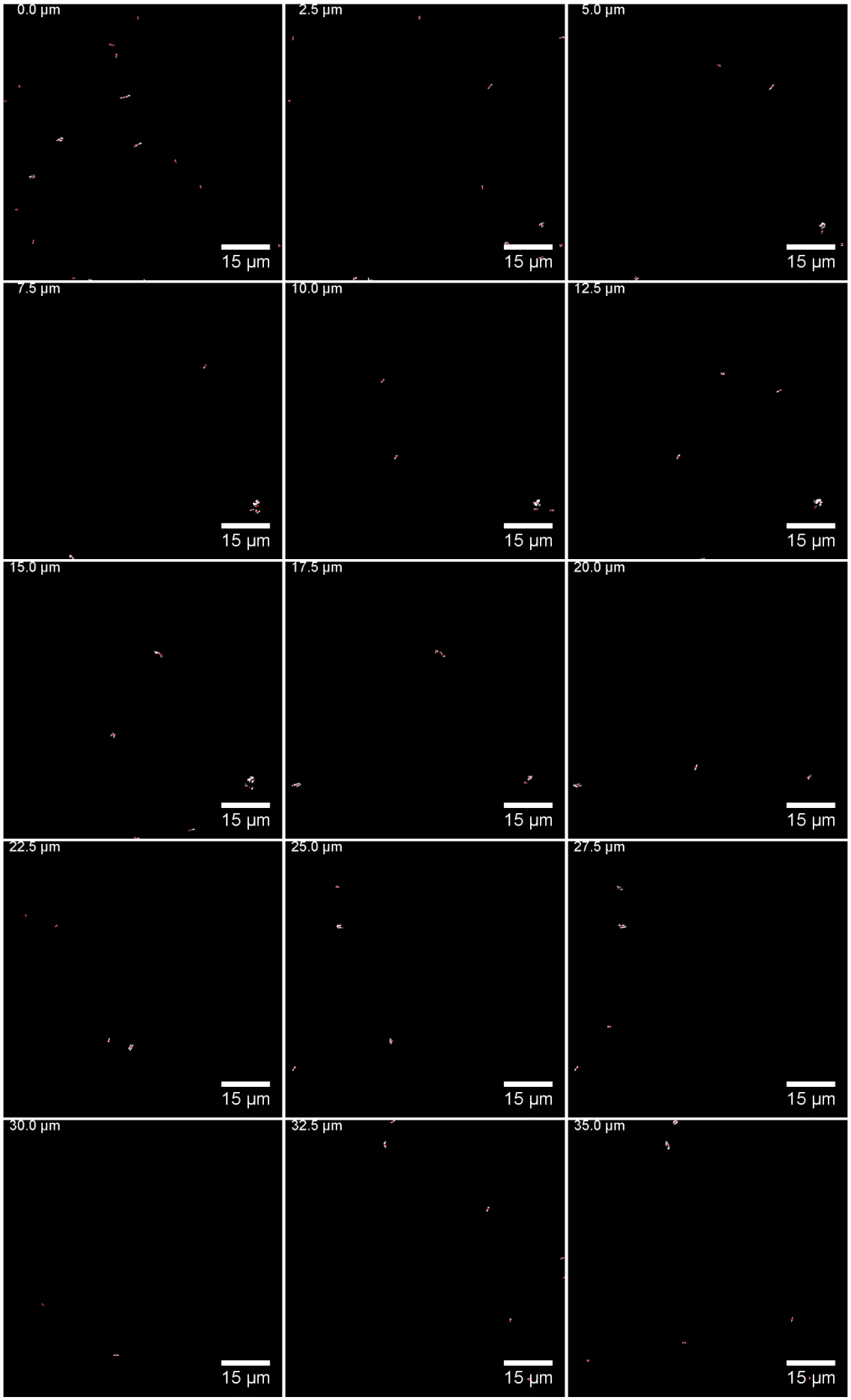
0.0 µm
15 µm
2.5 µm
15 µm
5.0 µm
15 µm
7.5 µm
15 µm
10.0 µm
15 µm
12.5 µm
15 µm
15.0 µm
15 µm
17.5 µm
15 µm
20.0 µm
15 µm
22.5 µm
15 µm
25.0 µm
15 µm
27.5 µm
15 µm
30.0 µm
15 µm
32.5 µm
15 µm
35.0 µm
15 µm

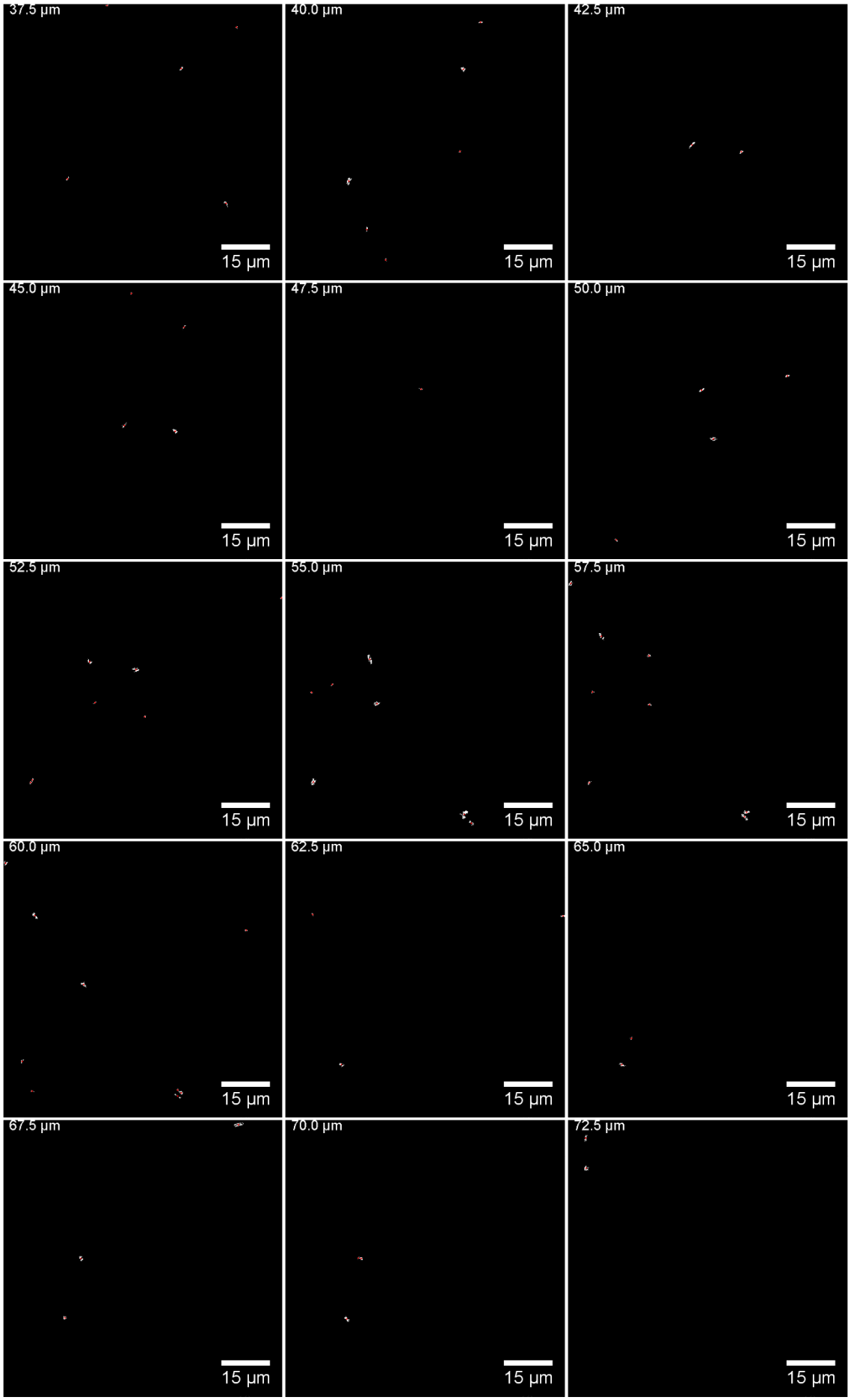
37.5 µm
15 µm
40.0 µm
15 µm
42.5 µm
15 µm
45.0 µm
15 µm
47.5 µm
15 µm
50.0 µm
15 µm
52.5 µm
15 µm
55.0 µm
15 µm
57.5 µm
15 µm
60.0 µm
15 µm
62.5 µm
15 µm
65.0 µm
15 µm
67.5 µm
15 µm
70.0 µm
15 µm
72.5 µm
15 µm

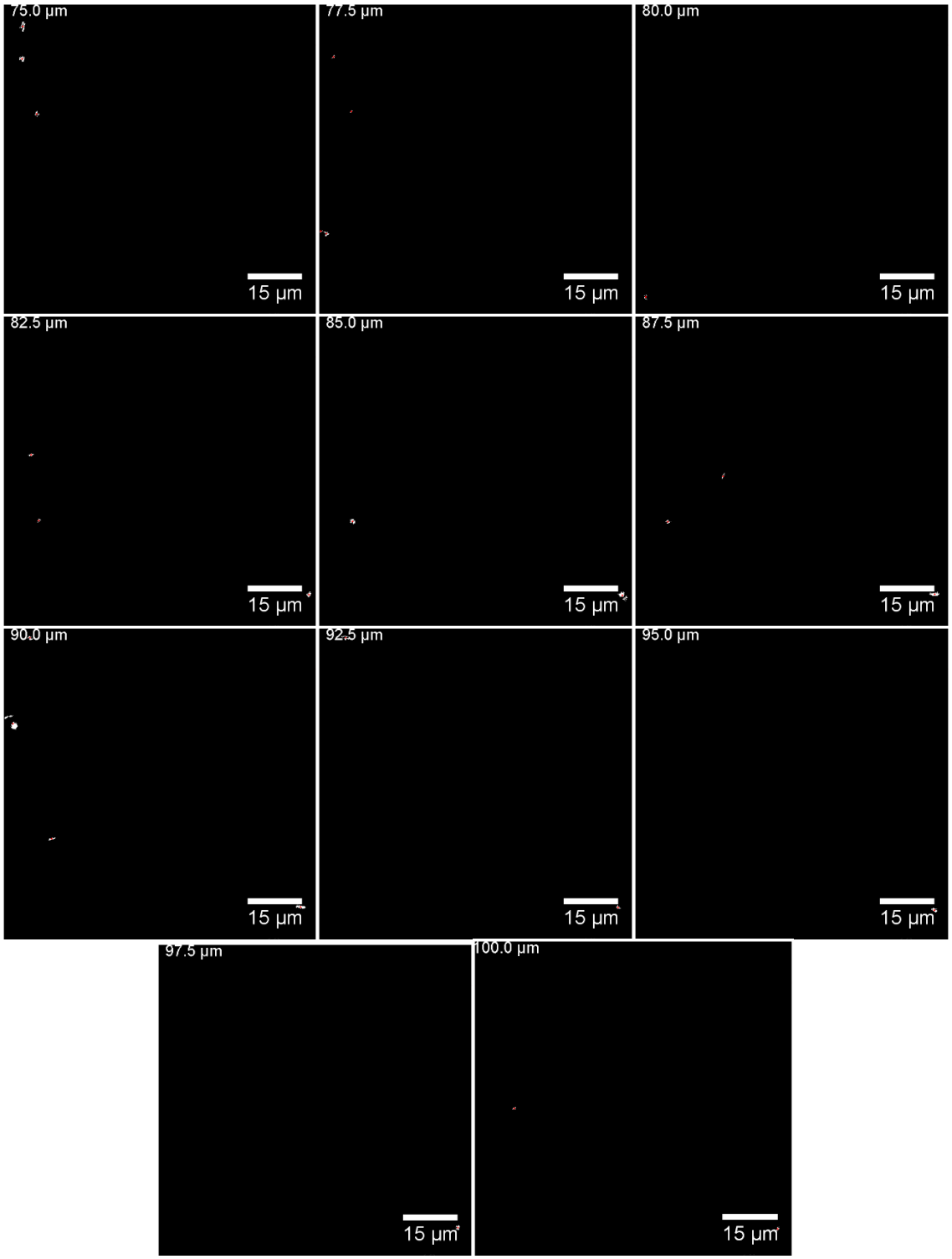


Figure SI5. DIC images of bacteria through multiple z-stacks. Images shown have been binarised based upon a set threshold (2× the standard deviation of the background pixel intensity) to highlight cells in white. The calculated zero order moment of inertia is shown as a red dot. The position of the DIC image within the z-stack is indicated in the top left corner.

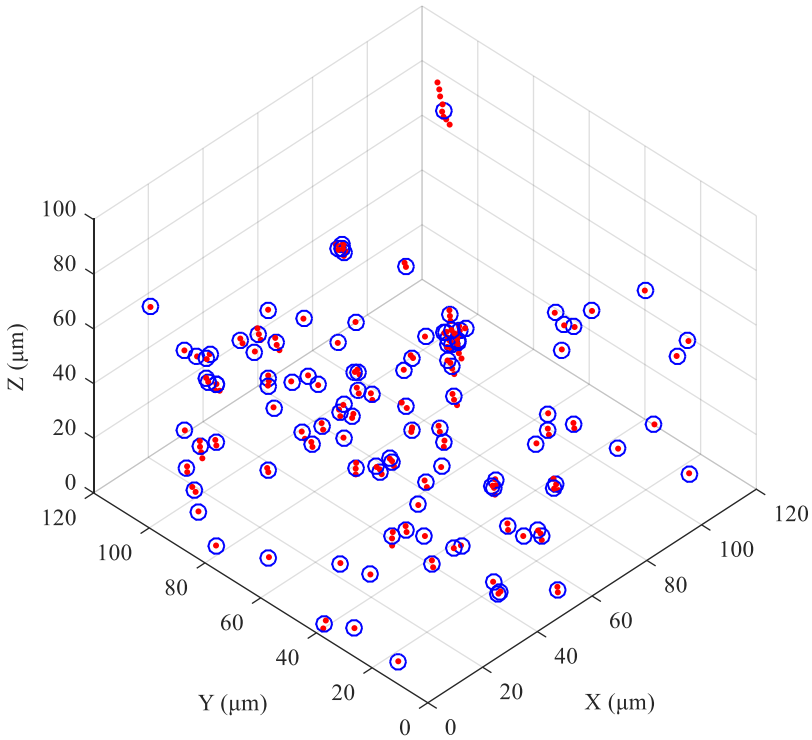


Figure SI6. Image showing particle detection across frames using bespoke Matlab script StackMaster. Red dots show objects identified on each frame and blue circles show the zero-order moment of inertia calculated for an object using combined pixels across frames.

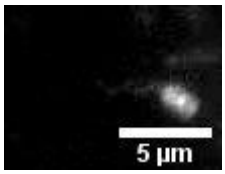


Figure SI7. TIRF image of *P. aeruginosa* wild-type bacterium stained with AlexaFluor 488 to enable visualisation of the flagella. The coiled flagella length was measured to be 3.8 µm.

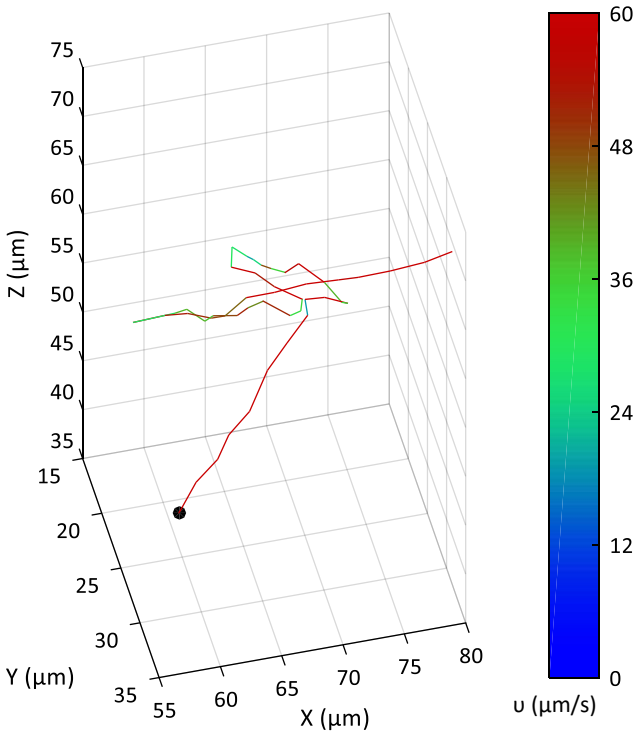


Figure SI8. Example of run-reverse trajectory. The start of the trajectory is indicated by a black dot. The track is coloured by the instantaneous speed according to the intensity scale.

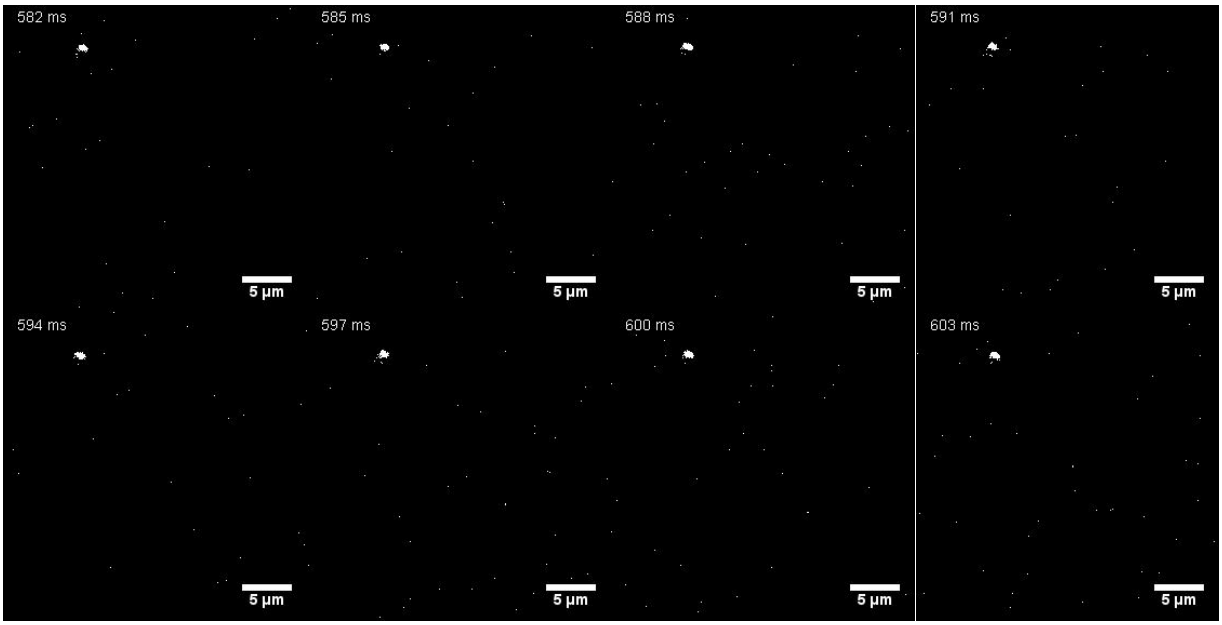


Figure SI9. DIC image sequence at high frame rate (333 Hz) of PA wildtype cell first swimming to the left and then reversing to travel to the right. Images have been binarised to improve visibility. See also supplementary video 3 for full image sequence.

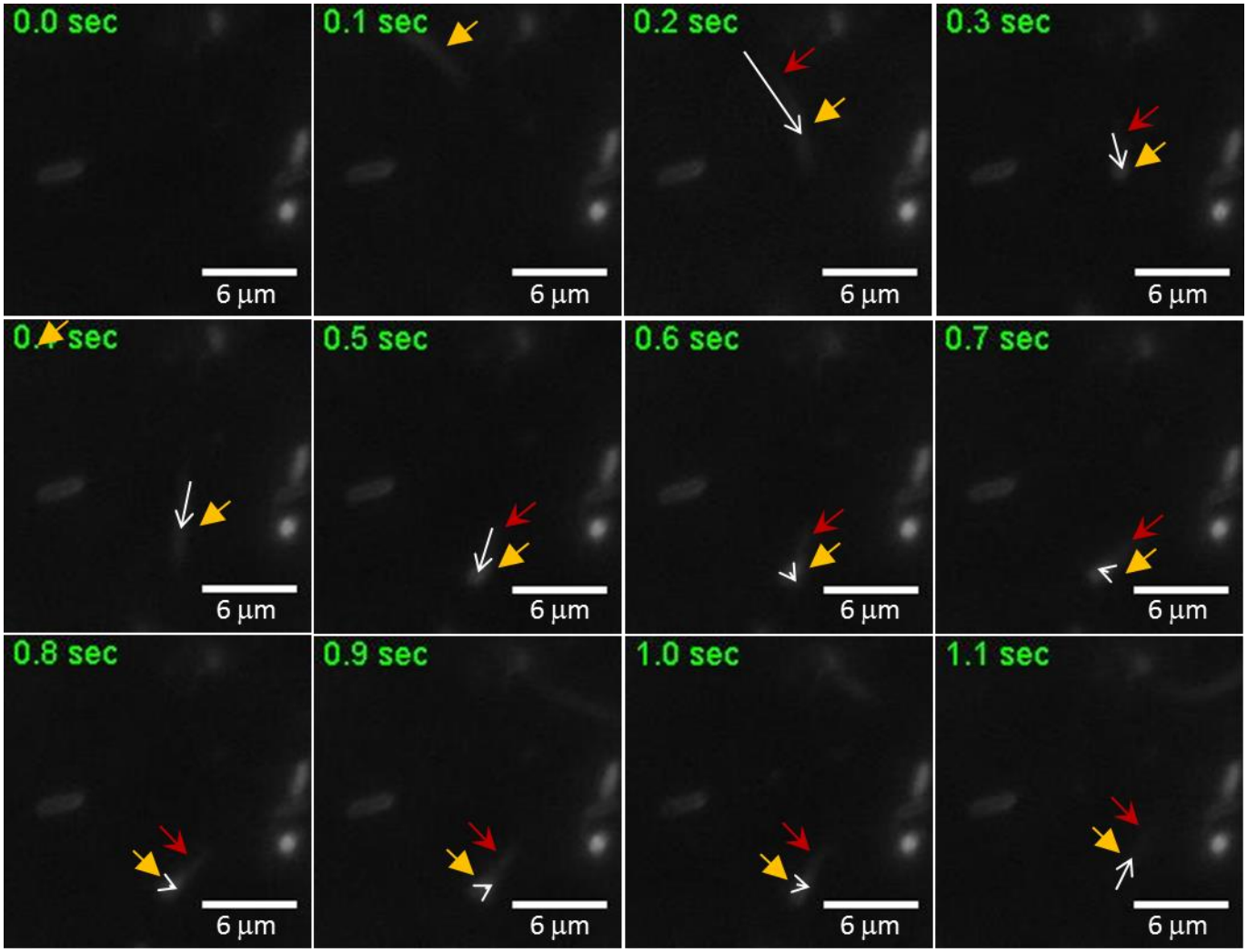


Figure SI10. TIRF image sequence using a 488 nm laser excitation and showing *P. aeruginosa* wild-type arriving and then leaving the surface, demonstrating push and pull swimming behaviour. TIRF evanescent field thickness set to 300 nm. Image capture at 10 Hz using a 60×, NA=1.4 objective. The white arrow show the displacement vector between the centre of mass of the bacterial cell of interest between two frames. The yellow arrow identifies the centre of mass of the body and the red arrow shows the position of the flagella (when visible) of the bacterial cell of interest. All other cells in the frame were stationary for the duration of the image sequence.

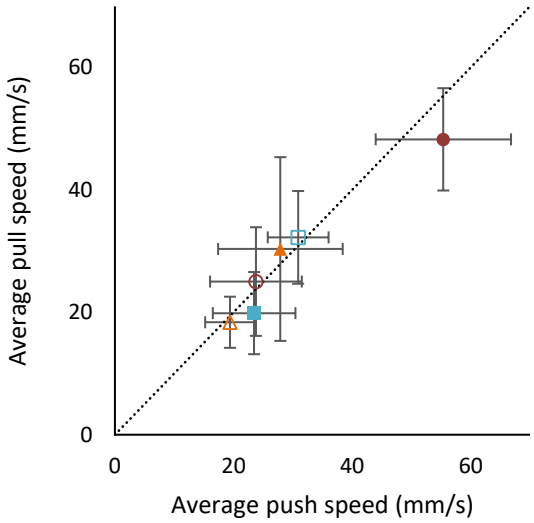


Figure SI11. Comparison of push and pull speeds of *P. aeruginosa* wildtype (circles) with *motAB* (triangles) and *motCD* (squares) mutants in the bulk (closed) and at the surface (open). Error bars represent 95% confidence limits.

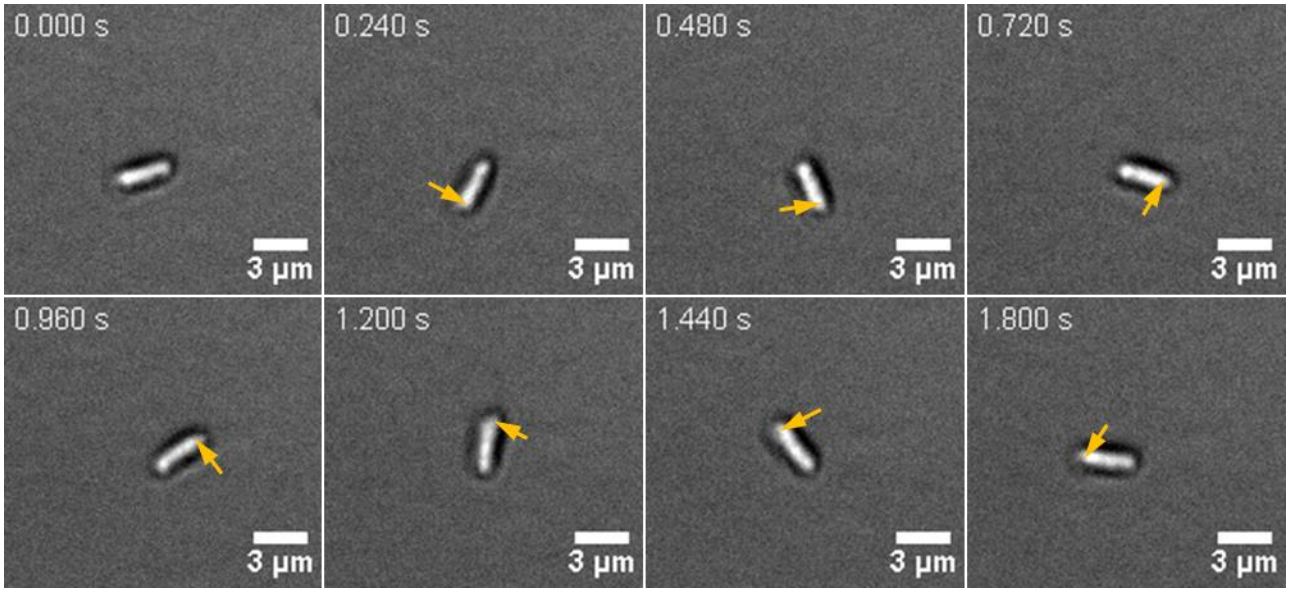


Figure SI12. DIC image sequence showing a spinning *P. aeruginosa* cell. Golden arrow indicates rotational movement of bacteria. Time intervals between images shown is 240 ms. See also supplementary video 5.

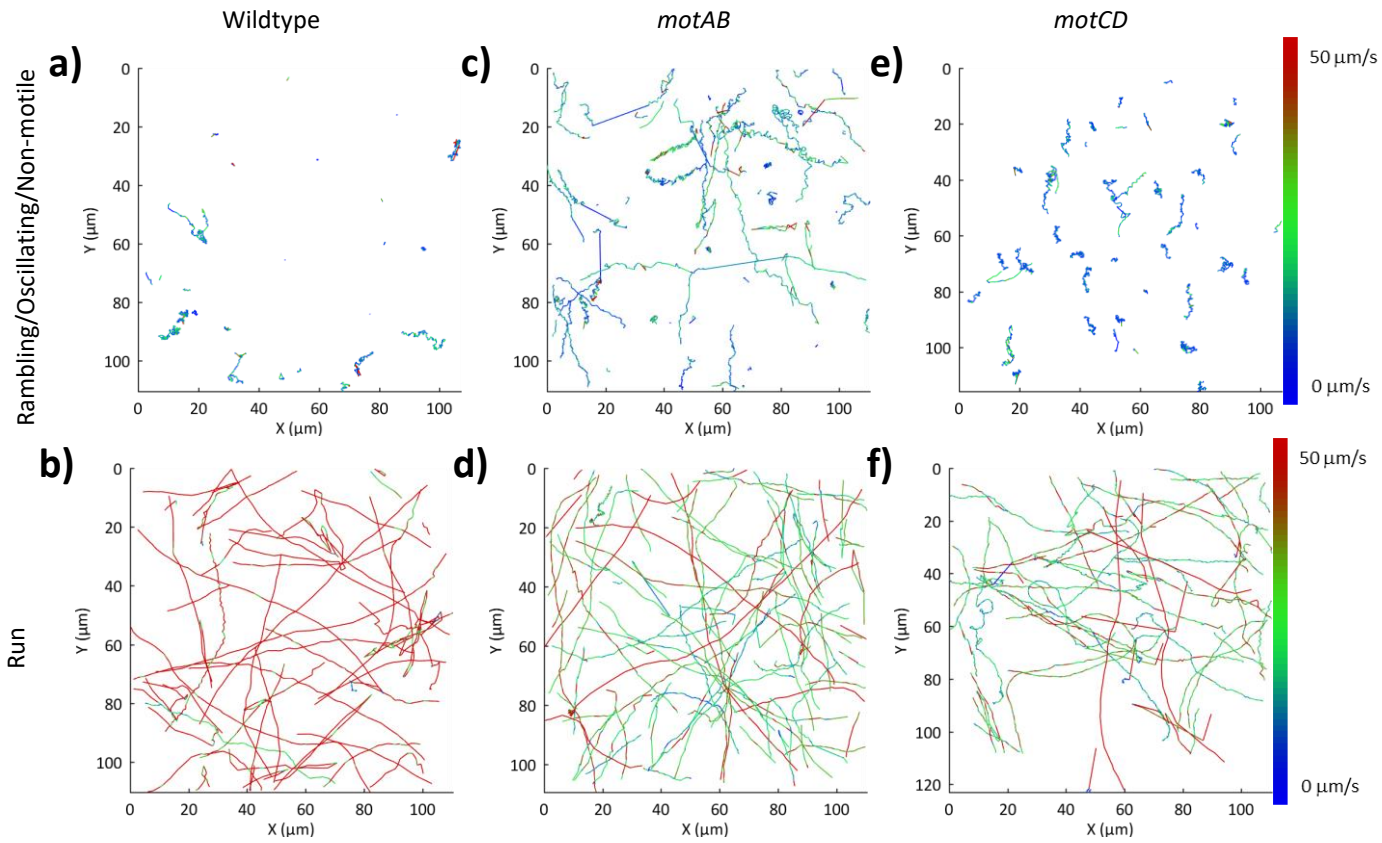


Figure SI13. Bacterial trajectories for *P. aeruginosa* (**a-b**) wildtype, (**c-d**) *motAB*, and (**e-f**) *motCD* mutants, showing the trajectories coloured based upon the speed according to the intensity scale from a top view (left) and all associated objects where the object volume is indicated by the size of the marker from an isometric view (right). Trajectories have been split into rambling (**a,c,e)** and swimming (**b,d,f**,) trajectories.

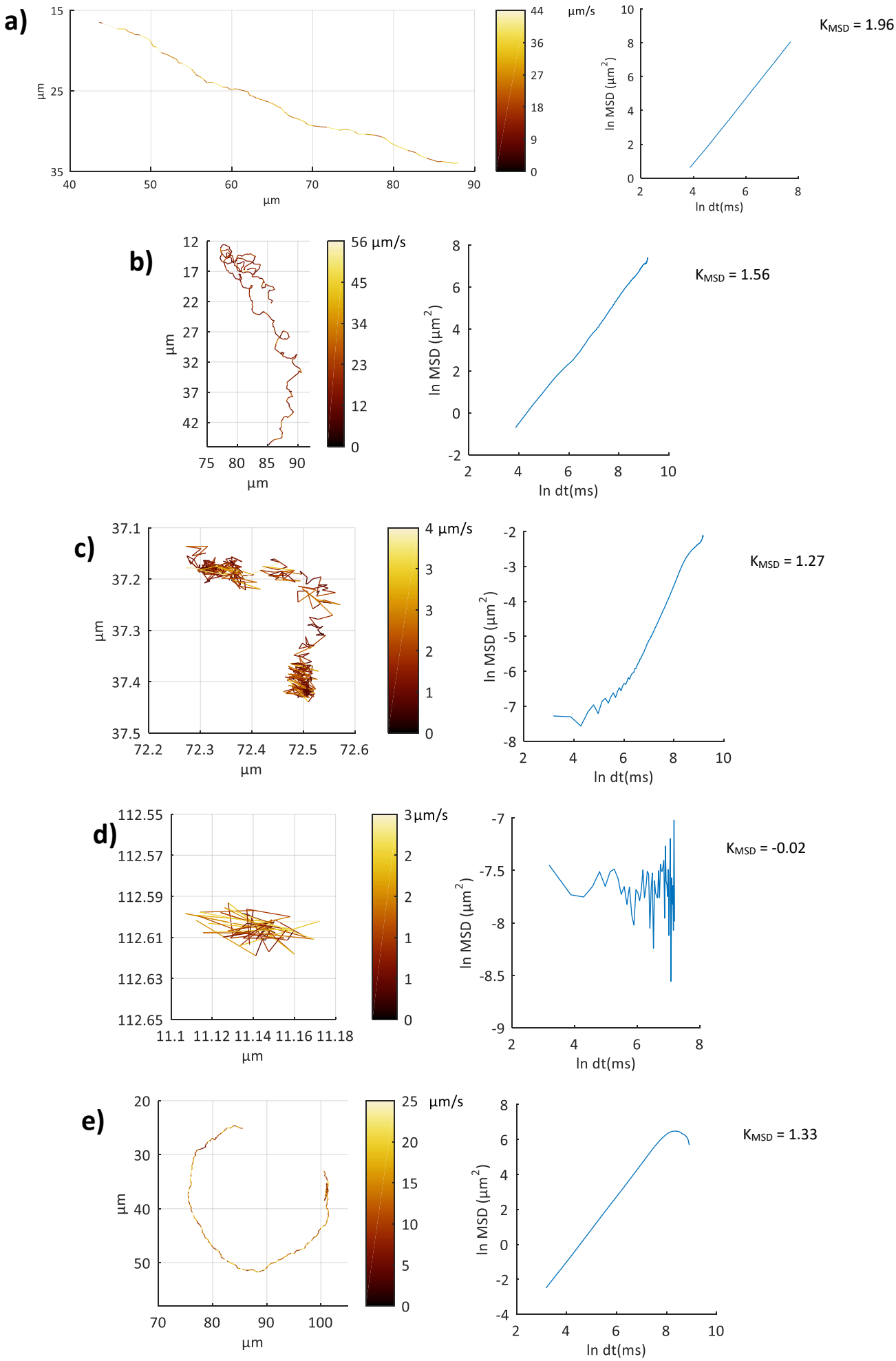
a)
µm
µm
µm/s
ln MSD (µm²)
ln dt(ms)
K_MSD = 1.96
b)
µm
µm
56 µm/s
ln MSD (µm²)
ln dt(ms)
K_MSD = 1.56
c)
µm
µm
4 µm/s
ln MSD (µm²)
ln dt(ms)
K_MSD = 1.27
d)
µm
µm
3µm/s
ln MSD (µm²)
ln dt(ms)
K_MSD = -0.02
e)
µm
µm
µm/s
ln MSD (µm²)
ln dt(ms)
K_MSD = 1.33

*Figure SI14 continued on next page.*

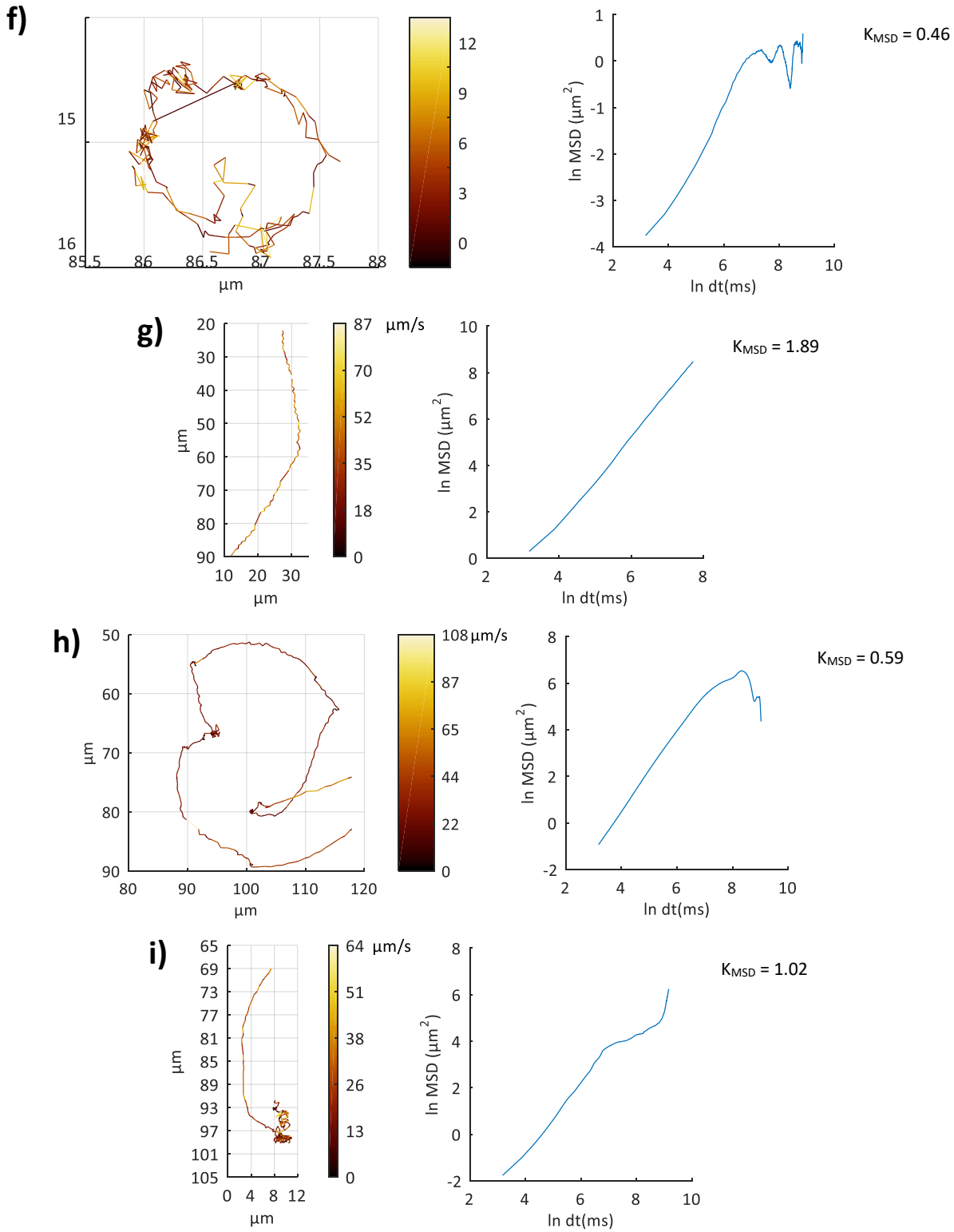


Figure SI14. Examples of different track types, showing the X,Y position of the track (left) and the log-log plot of MSD at various time intervals dt (right). The X,Y coordinates of the track have been coloured according to the tracks instantaneous speed according to the intensity map provided in units of µm/s. The slope of the line of best fit through the log-log plot is shown ($K_{MSD}$)[1]

[1] $K_{MSD}$ has widely been used to characterise the movement of particles, enabling directed, Brownian and confined movement to be defined. A number of different examples of bacterial tracks and the associated $K_{MSD}$ measurements are shown in Figure SI14. Tracks travelling directionally were observed to produce a linear relationship between the log of MSD over the log of time intervals with a slope approaching 2 (Figure SI14a). A track characterised by frequent oscillations had a reduced $K_{MSD}$ of 1.56 (Figure SI14b), whilst the drifting of a non-motile bacterium had a $K_{MSD}$ closer to 1 (Figure SI14c). A bacterium attached to the surface and therefore confined has a $K_{MSD}$ of approximately 0 (Figure SI14d). A $K_{MSD}$ below 2 was also observed for a bacterium travelling in circular trajectories (Figure SI14e) or spinning (Figure SI14f). In this case a linear relationship between the ln of MSD and ln of $\delta t$ was observed up to the time interval associated with a complete oscillation, whereupon a plateau in the log MSD was observed at a position determined by the diameter of the curved path (Figure SI14f). In cases where the

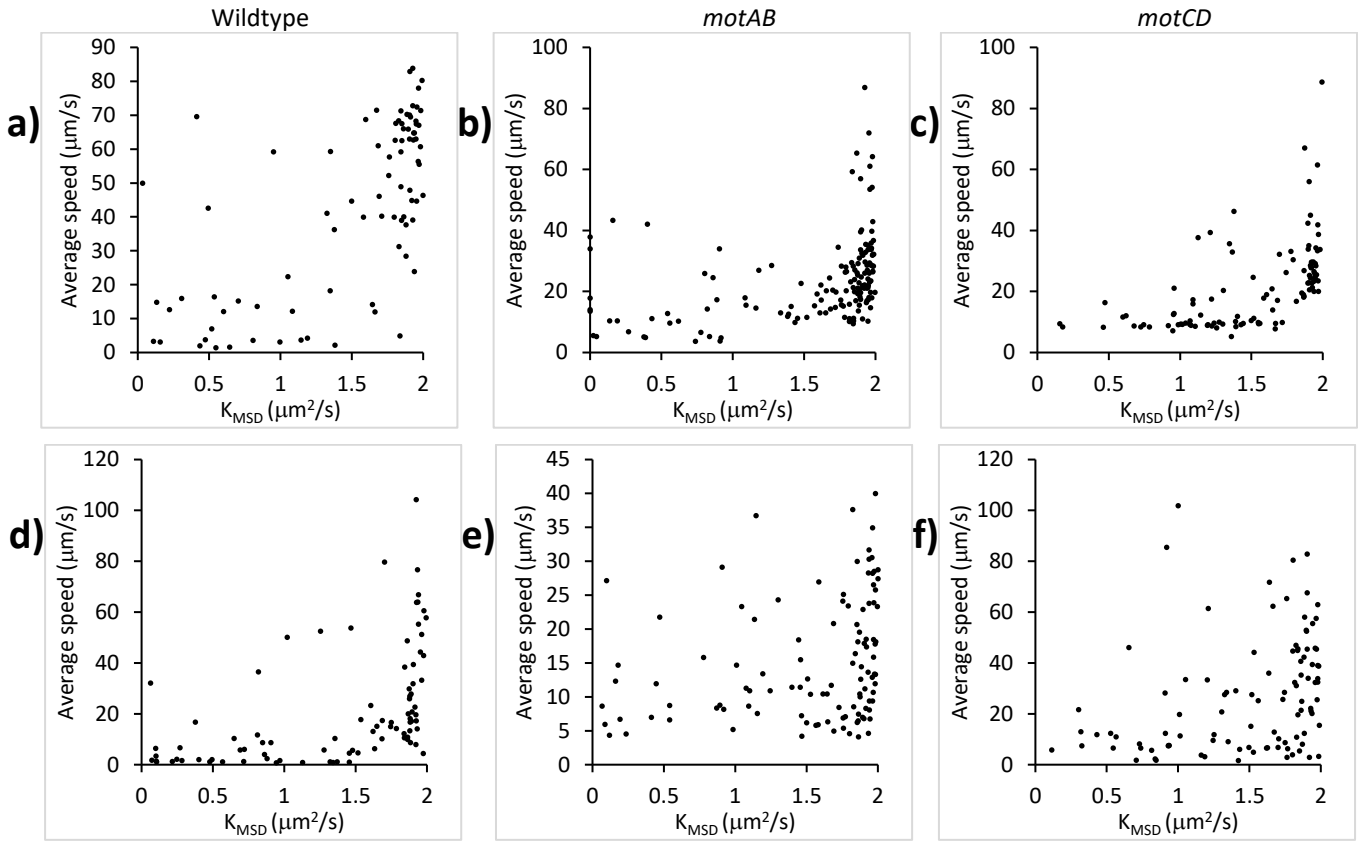


Figure SI15. Plot of the mean speed (µm/s) and $K_{MSD}$ for every track measured in the bulk (**a-c**) and at the surface (**d-f**) for (**a and d**) wildtype, (**b** and **e**) *motAB* and (**c** and **f**) *motCD* mutants from 4 biological replicates.

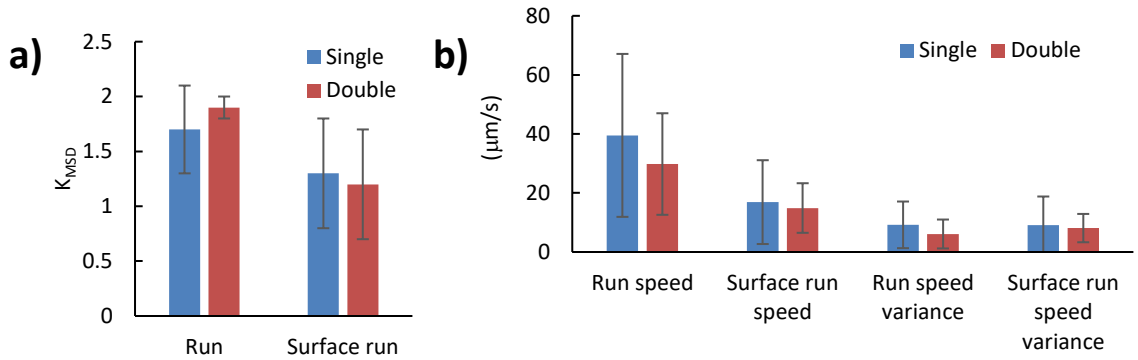


Figure SI16. Comparison of the run trajectories for single cells (■) and cells in the process of cell division (double) (■). a) The $K_{MSD}$ values calculated for runs and surface runs for single and dividing cells. Error bars are equal to ± 1 standard deviation unit, N=5. b) Comparison of average speed of runs and surface runs for single and dividing cells. Run speed variance is the average standard deviation for the instantaneous speeds measured for an entire trajectory. Error bars are equal to ± 1 standard deviation unit, N=5.

bacterium experienced oscillating movement over short time scales (fluctuating motion) and directional movement over larger times scales (mean motion) two slopes were observed on the log-log plot of MSD and δt (Figure SI14g), whereupon the two slopes were indicative of the directionality of the two movement types. As directional movement of the bacteria was of interest for comparing trajectories and the oscillating movement of the bacteria over short time frames was undersampled (Figure SI4) the $K_{MSD}$ value was calculated over δt values of 50 to 1000 ms. Changes in the bacterial movement during a single track caused by reversal events or attachment or detachment events resulted in spurious measurements of $K_{MSD}$ (Figure SI14h-j). For this reason tracks were split when attachment, detachment or reversal events were observed prior to $K_{MSD}$ analysis.

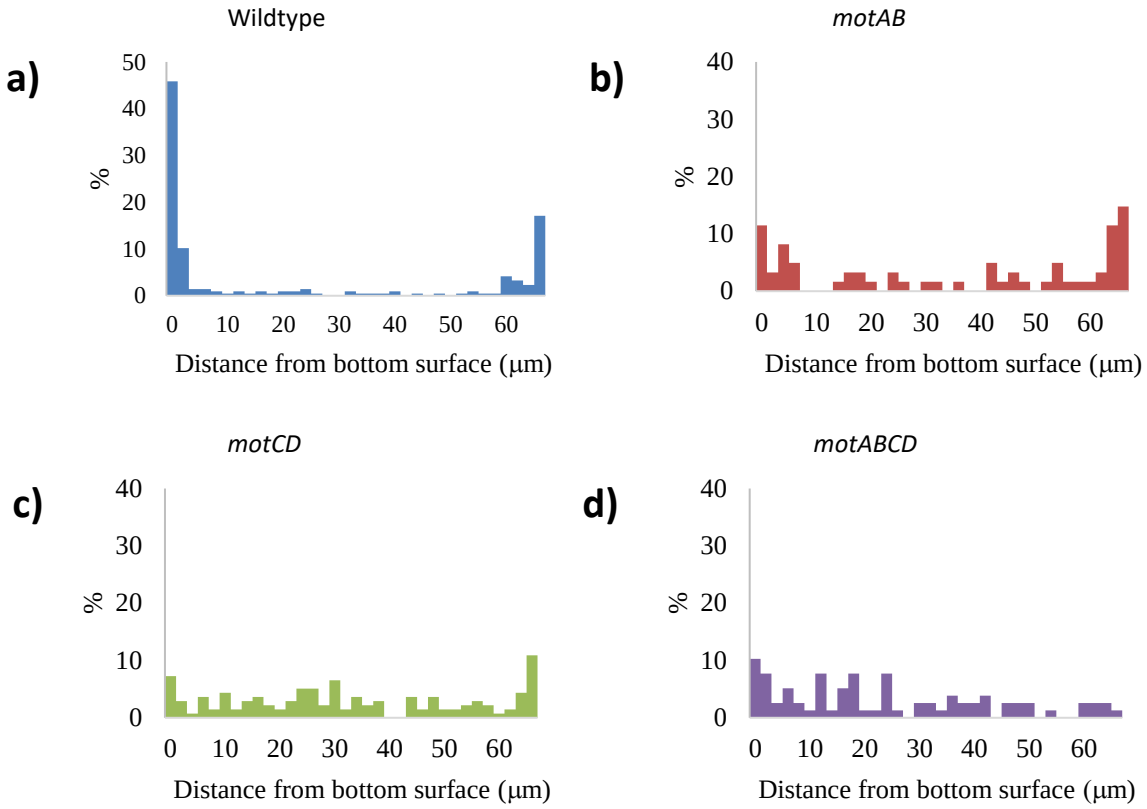


Figure SI17. Positions of bacteria within a glass sandwich taken approximately 5 min after addition to chamber. *P. aeruginosa* (**a**) wild-type, (**b**) *motAB*, (**c**) *motCD* and (**d**) *motABCD* mutants. Data presented as a % of total number of cells observed in the z-stack. Example stacks from each strain are shown in Figure SI19.

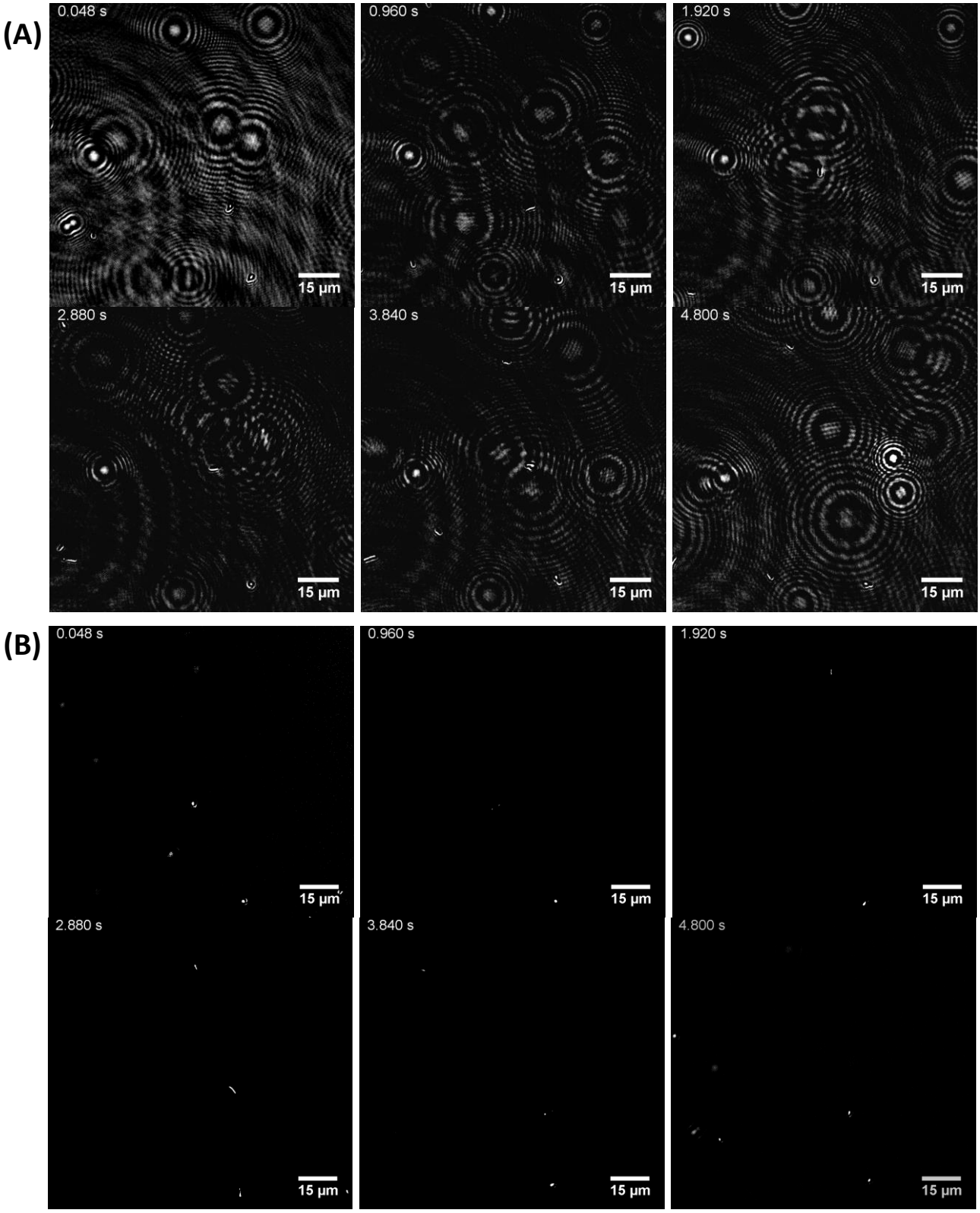


Figure SI18. Image sequence related to Figure SI3 showing corresponding (**A**) DHM and (**B**) DIC images for *P. aeruginosa* wildtype captured at time points of 0.048, 0.960, 1.920, 2.880, 3.840 and 4.80 s.

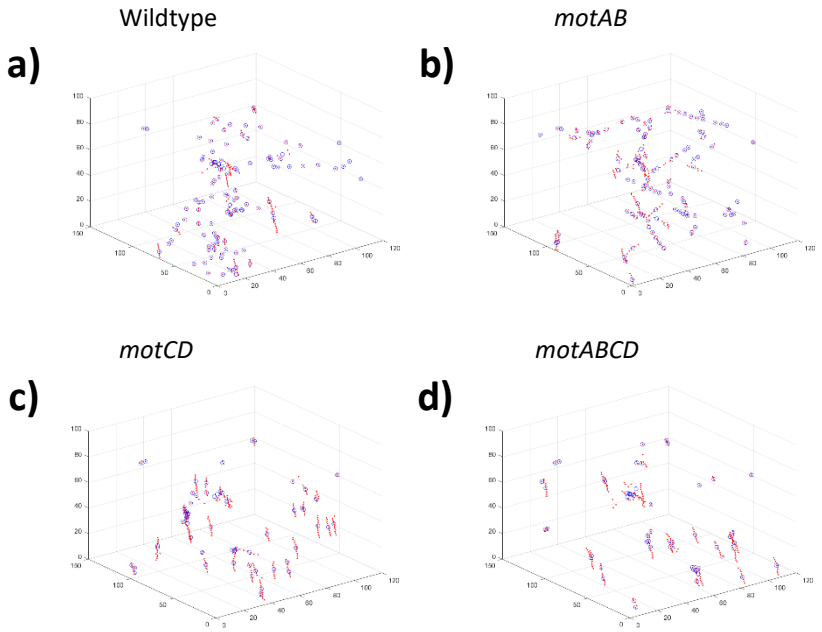


Figure SI19. Scatter plots of all detected objects (red dots) and objects assigned as bacteria (blue circles) for DIC z-stacks for *P. aeruginosa* (a) wildtype and (b) *motAB*, (c) *motCD*, (d) *motABC* mutants. Axis dimensions in microns.

Table SI1. List of oligonucleotides used in this study for the construction of *motAB* and *motCD* in frame deletion mutants and for genetic complementation.

| Name | Sequences |
|---|---|
| **MotABΔ FW1** | 5'-ATATCTAGAAGTTGGCTCGCGCGTCCCAG-3' |
| **MotABΔ RV1** | 5'-TCAGTCGCCCTTGATGATTTTTGACATGAGGACCGG-3' |
| **MotABΔ FW2** | 5'-CTCATGTCAAAAATCATCAAGGGCGACTGAGGTTCA-3' |
| **MotABΔ RV2** | 5'-TATAAGCTTTGGTGAATGCCTTGTTGCCA-3' |
| **MotCDΔ FW1** | 5'-ATATCTAGAAGCAGATGATGGTCGACGGC-3' |
| **MotCDΔ RV1** | 5'-TCATGGCGAAGGCGAGAGCACATCCATCAGCGCGTC-3' |
| **MotCDΔ FW2** | 5'-CTGATGGATGTGCTCTCGCCTTCGCCATGAGCGCGC-3' |
| **MotCDΔ RV2** | 5'-TATAAGCTTAGGCTCTTCGAGACCACCAG-3' |
| **MotAB FW** | 5'-TATGAATTCATGTCAAAAATCATCGGC-3' |
| **MotAB RW** | 5'-TATCTCGAGTCAGTCGCCCTTGATCTG-3' |
| **MotCD FW** | 5'-TATGAATTCATGGATGTGCTCAGCCTG-3' |
| **MotCD RW** | 5'-TATCTCGAGTCATGGCGAAGGCGACGG-3' |